5-12-2008

# ATF4 Is an Oxidative Stress–Inducible, Prodeath Transcription Factor in Neurons in Vitro and in Vivo

Philipp Lange

Juan Chavez

John T. Pinto
*New York Medical College*

Giovanni Coppola

Chiao-Wang Sun

*See next page for additional authors*



## Recommended Citation

Lange, P. S., Chavez, J. C., Pinto, J. T., Coppola, G., Sun, C., Townes, T. M., . . . Ratan, R. R. (2008). ATF4 is an oxidative stress–inducible, prodeath transcription factor in neurons in vitro and in vivo. The Journal of Experimental Medicine, 205(5), 1227-1242. doi:10.1084/jem.20071460

Published May 5, 2008



# ATF4 is an oxidative stress–inducible, prodeath transcription factor in neurons in vitro and in vivo

Philipp S. Lange,[1,2,9] Juan C. Chavez,[1,2,3] John T. Pinto,[4] Giovanni Coppola,[6] Chiao-Wang Sun,[8] Tim M. Townes,[8] Daniel H. Geschwind,[5,6,7] and Rajiv R. Ratan[1,2]

[1]Burke Medical Research Institute, White Plains, NY 10605
[2]Department of Neurology and Neuroscience, Weill Medical College of Cornell University, New York, NY 10021
[3]Discovery Translational Medicine, Wyeth Research, Collegeville, PA 19426
[4]Department of Biochemistry and Molecular Biology, New York Medical College, Valhalla, NY 10595
[5]Department of Human Genetics, [6]Program in Neurogenetics, Department of Neurology, and [7]Semel Institute, David Geffen School of Medicine, University of California, Los Angeles, Los Angeles, CA 90095
[8]Department of Biochemistry and Molecular Genetics, School of Medicine and School of Dentistry, University of Alabama at Birmingham, Birmingham, AL 35294
[9]Department of Anesthesiology and Intensive Care Medicine, University of Bonn, 53127 Bonn, Germany

**Oxidative stress is pathogenic in neurological diseases, including stroke. The identity of oxidative stress–inducible transcription factors and their role in propagating the death cascade are not well known. In an in vitro model of oxidative stress, the expression of the bZip transcription factor activating transcription factor 4 (ATF4) was induced by glutathione depletion and localized to the promoter of a putative death gene in neurons. Germline deletion of ATF4 resulted in a profound reduction in oxidative stress–induced gene expression and resistance to oxidative death. In neurons, ATF4 modulates an early, upstream event in the death pathway, as resistance to oxidative death by ATF4 deletion was associated with decreased consumption of the antioxidant glutathione. Forced expression of ATF4 was sufficient to promote cell death and loss of glutathione. In ATF4$^{-/-}$ neurons, restoration of ATF4 protein expression reinstated sensitivity to oxidative death. In addition, ATF4$^{-/-}$ mice experienced significantly smaller infarcts and improved behavioral recovery as compared with wild-type mice subjected to the same reductions in blood flow in a rodent model of ischemic stroke. Collectively, these findings establish ATF4 as a redox-regulated, prodeath transcriptional activator in the nervous system that propagates death responses to oxidative stress in vitro and to stroke in vivo.**

CORRESPONDENCE
Philipp S. Lange:
phl2006@med.cornell.edu
OR
Rajiv R. Ratan:
rratan@burke.org

Abbreviations used: ATF4, activating transcription factor 4; BHA, butylated hydroxyanisol; BSO, buthionine sulfoximine; DCF, 2′,7′-dichlorofluorescin; γ-GCS, γ-glutamylcysteine synthetase; HCA, homocysteate; MAP2, microtubule-associated protein 2; MCAo, middle cerebral artery occlusion; MOI, multiplicity of infection; ROS, reactive oxygen species; TRB3, tribbles homologue 3.

Free radicals and their reactive metabolites (reactive oxygen species [ROS]) exist in neuronal cells and tissues at low but measurable concentrations (1). These tolerable equilibrium concentrations are the result of a tightly controlled balance between the rates of production and clearance, the latter being mediated by a team of antioxidants including enzymes and nonenzymatic compounds such as the tripeptide glutathione.

Cells or tissues are in a stable oxidative state if the rates of ROS production and scavenging capacity remain within a homeostatic range. However, if this balance is disturbed, either by an increase in ROS concentrations or a decrease in antioxidant activities, the response may not be sufficient to keep the system at a level compatible with survival. In such cases, oxidants can modify cellular targets, leading to cell dysfunction or death (2). Indeed, oxidative stress has been implicated in virtually all of the major acute and chronic neurodegenerative diseases (3).

In many cells, including cortical neurons, the expression of genes with antioxidative activity is precisely controlled by a synergistic network of redox-sensing signaling cascades (4, 5). Specifically, aberrant levels of oxidants can trigger the transcriptional induction of antioxidative enzymes and other adaptive pathways (5).

The online version of this article contains supplemental material.

Published May 5, 2008



The cellular response to oxidative stress is tightly controlled by a family of stress-responsive transcription factors (2, 6). Among these transcription factors, the activating transcription factor 4 (ATF4)/cAMP response element binding protein 2 may be a key player (7–9). ATF4 is expressed constitutively only at low concentrations but becomes rapidly induced under particular cell-stress conditions (10). ATF4 binds to the promoter regions of an array of different target genes, including many involved in amino acid metabolism and redox control (11). In fibroblasts, ATF4 coordinates the response to amino acid depletion, oxidative stress, and endoplasmic reticulum stress, and helps to balance redox homeostasis. Indeed, ATF4-deficient fibroblasts have been shown to be prone to death after a host of stresses, including oxidative stress and amino acid deprivation (11).

Interestingly, amino acid deprivation has been previously reported to be neuroprotective in an in vitro model of oxidative stress–induced cell death (12). This model employs immature cortical neurons and takes advantage of the absence of glutamate receptors at this stage of development to avoid excitotoxicity. Instead, addition of glutamate analogues competitively inhibits uptake of cyst(e)ine, the rate-limiting precursor for the tripeptide glutathione. The resulting decline in glutathione concentration is a primary event that leads to neuronal cell death from oxidative stress (13–15), a process that displays many features of apoptosis (14–16). This glutathione depletion model facilitates the separation of biochemical events that mediate death from those that are a consequence of death, and it is highly relevant to pathological conditions because an increase in cellular ROS production is often observed in apoptotic processes triggered by diverse stimuli associated with disease states. In this work, we define a novel prodeath role for ATF4 in neurons in vitro in response to oxidative stress and in vivo in response to stroke, a condition linked to oxidative stress.

## RESULTS

### Amino acid depletion and thapsigargin treatment induce ATF4 and protect embryonic cortical neurons from oxidative stress–induced cell death

Amino acid depletion via the arginine-degrading enzyme arginase is a well-characterized strategy for protecting neurons from oxidative stress–induced cell death (12, 17). Studies in nonneural cells have shown that amino acid deprivation activates cell-survival pathways by activating the bZip transcription factor ATF4 (11). We initiated our studies with the hypothesis that arginase is a multipotent inhibitor of apoptotic neuronal cell death by activating ATF4 and its downstream gene targets. Because endoplasmic reticulum stress by thapsigargin is also associated with increased ATF4 expression (18), we examined the corollary hypothesis that this agent could initiate tolerance to oxidative stress in primary cortical neurons. As predicted, arginase and thapsigargin led to nearly complete protection from neuronal cell death (Fig. 1, A and B) and to accumulation of ATF4 protein (Fig. 1 C). Interestingly, we found that oxidative stress alone was sufficient to induce ATF4 protein levels (Fig. 1 C).

### Cortical neurons from ATF4$^{-/-}$ brains are resistant to oxidative stress–induced cell death

To verify that the protection by arginase and thapsigargin requires ATF4, we cultured cortical neurons from brains of embryonic ATF4$^{-/-}$ mice (E15.5). Immunohistochemical analysis (Fig. 2 A) using an antibody to microtubule-associated protein 2 (MAP2; which stains neural dendrites) showed that basal viability and morphology of cell bodies and dendrites did not display any differences between ATF4$^{+/+}$ and ATF4$^{-/-}$ neurons. We found that ATF4 mRNA was induced in ATF4$^{+/+}$ neurons after oxidative stress and confirmed its absence in ATF4$^{-/-}$ neurons (Fig. 2 B). We then examined susceptibility to oxidative stress induced by the glutamate analogue homocysteate (HCA) in ATF4$^{+/+}$ and ATF4$^{-/-}$ cortical neurons (Fig. 2, C and D). Contrary to our hypothesis, we found that ATF4$^{-/-}$ neurons were significantly protected from oxidative stress–induced death. ATF4$^{-/-}$ neurons demonstrated enhanced resistance, as monitored by MTT reduction (Fig. 2 C) and live/dead staining (Fig. 2 D). Moreover, in ATF4$^{+/+}$ neurons, ATF4 induction by treatment with HCA was a result of induction at the translational level (Fig. 2 E). We confirmed the nuclear accumulation of ATF4 in ATF4$^{+/+}$ neurons exposed to oxidative stress (Fig. 2 F). Higher nuclear ATF4 activity after oxidative stress was demonstrated by showing higher promoter activity of an ATF4 target gene, tribbles homologue 3 (TRB3), that has been recently associated with cell death. TRB3 mRNA is induced upon HCA treatment in an ATF4-dependent manner (Fig. 2 G). To characterize ATF4 binding on the promoter of TRB3, we generated a 2-kb fragment of the mouse TRB3 promoter (Fig. 2 H). This fragment contains a 33-bp element whose human analogue has been characterized as a DNA binding region of ATF4. Transfection of both ATF4$^{+/+}$ and ATF4$^{-/-}$ neurons with the TRB3WT promoter construct, along with a mutant version lacking the binding element, revealed that this element plays an important but not exclusive role in the induction of the TRB3 promoter after oxidative stress. In the absence of ATF4, the TRB3 promoter activity was not induced in response to oxidative stress.

### Microarray analysis reveals that ATF4 regulates a subset of genes that are induced in response to oxidative stress

In fibroblasts, previous studies (11) have established ATF4 as an important prosurvival transcription factor in the context of oxidative stress. Microarray analysis in that study (11) showed that several ATF4-regulated genes in fibroblasts are involved in amino acid import, glutathione biosynthesis, antioxidant defense, and DNA repair. In contrast, in neurons, ATF4 has classically been thought to act mainly as a transcriptional repressor. In this context, ATF4 has been hypothesized to negatively influence survival by repressing expression of genes that are otherwise activated by prosurvival transcriptional activators such as cAMP response element binding protein.

Published May 5, 2008



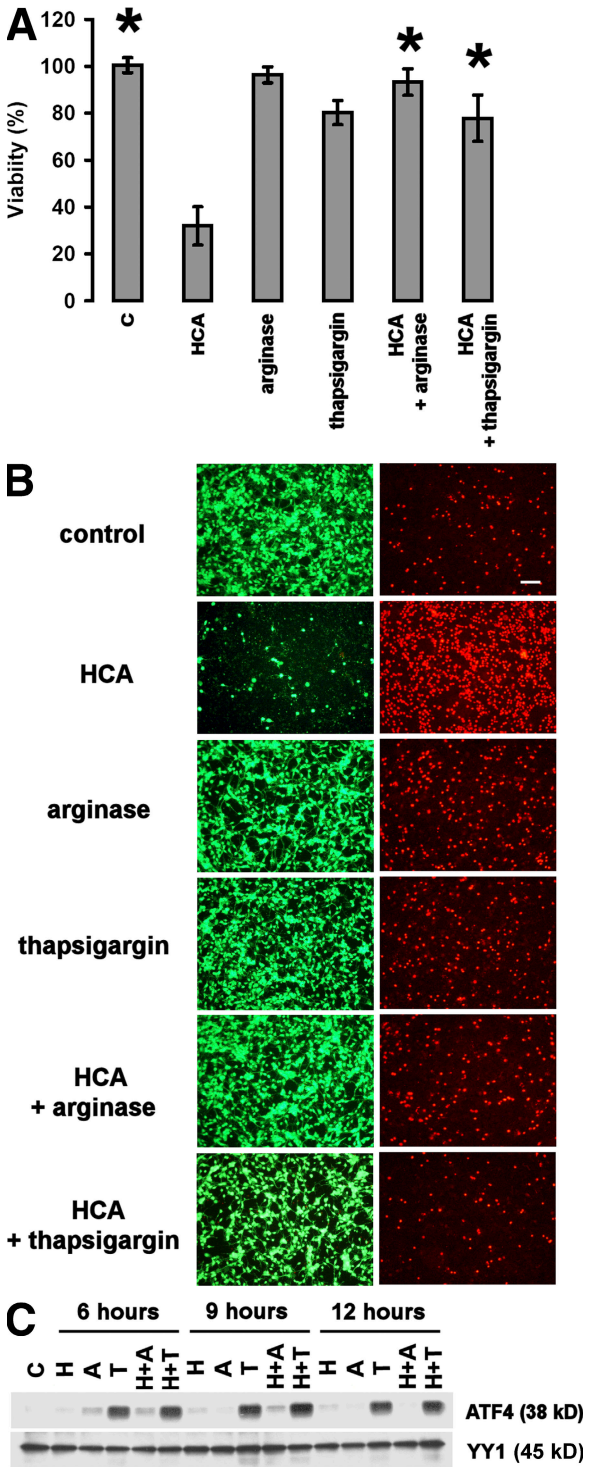


**Figure 1. Amino acid depletion and thapsigargin treatment induce ATF4 and protect embryonic cortical neurons from oxidative stress–induced cell death.** (A) Cortical neuronal cultures (1 d in vitro) were treated with a vehicle control (shown as C), 10 mM of the glutamate analogue HCA, 1 µg/ml arginase, 1 µM thapsigargin, 1 µg/ml arginase and 10 mM HCA, or 10 mM HCA and 1 µM thapsigargin. 24 h later, cell viability was determined using the MTT assay. The graph depicts mean (compared with control) ± SD calculated from three separate experiments for each group ($n = 25$). *, $P < 0.05$ from HCA-treated cultures by the Kruskal-Wallis test followed by Dunn's multiple comparisons test. (B) Live/dead assay of cortical neuronal cultures (2 d in vitro). Live cells were detected by uptake and trapping of calcein-AM (green fluorescence). Dead cells failed to trap calcein but were freely permeable to the highly charged DNA intercalating dye ethidium homodimer (red fluorescence). Bar, 50 µm. (C) Treatment with 10 mM HCA (shown as H) and 1 µg/ml arginase (shown as A) or 1 µM thapsigargin (shown as T), alone or in combination with HCA, increases the expression of ATF4 in cultured cortical neurons as compared with vehicle-treated control (shown as C). Cells were harvested at the indicated time points, and nuclear extracts were separated using gel electrophoresis and immunodetected using an antibody against ATF4. YY1 was monitored as a loading control. The immunoblot is a representative example of three experiments.

To begin to examine whether ATF4 functions primarily as a repressor or activator in neurons and to determine the extent to which these ATF4-regulated genes function similarly in fibroblasts and neurons, we performed a global analysis of gene expression using microarrays in $ATF4^{+/+}$ and $ATF4^{-/-}$ neurons (Fig. 3 A). More specifically, we assessed (a) the physiological genomic effect of ATF4 knockout (comparing $ATF4^{-/-}$ with $ATF4^{+/+}$ neurons), and (b) the effect of ATF4 knockout on the response to oxidative stress (comparing $ATF4^{-/-}$ with $ATF4^{+/+}$ neurons after HCA treatment; Fig. 3 B and Table I). At the chosen statistical threshold (5% false discovery rate), 136 probes were down-regulated in $ATF4^{-/-}$ versus $ATF4^{+/+}$ neurons, compared with 53 that were up-regulated, suggesting a role for ATF4 as a transcriptional activator. Functional gene ontology categories overrepresented in this list include mitochondrion, oxidoreductase activity, and amino acid metabolism. Several of the down-regulated genes have been shown to be positively regulated by ATF4, including the prodeath gene TRB3. Comparison of $ATF4^{-/-}$ versus $ATF4^{+/+}$ neurons after oxidative stress with HCA treatment suggested a fundamental role of ATF4 in modulating oxidative stress–induced gene expression. In fact, 119 probes are dysregulated in response to oxidative stress in $ATF4^{+/+}$ neurons, whereas only 3 change in $ATF4^{-/-}$ neurons. Collectively, these findings suggest that ATF4 is a major upstream regulator of oxidative stress–induced changes in gene expression. Additionally, for most genes in embryonic cortical neurons, ATF4 functions as an activator and not a repressor.

Gene expression array data were obtained from $ATF4^{-/-}$ fibroblasts that display a higher susceptibility to oxidative stress (11). A significant overlap could be observed between the array data from $ATF4^{-/-}$ fibroblasts and neurons (Table S1, available at http://www.jem.org/cgi/content/full/jem.20071460/DC1), indicating that ATF4 regulates at least a major part of target genes in a cell type–independent manner. These similarities do not explain the observation that ATF4 is prosurvival in fibroblasts and prodeath in neurons, but they demonstrate the reliability in our analysis. In contrast, a subset of genes, including the prodeath gene TRB3, were ATF4-regulated in neurons but not in fibroblasts. Collectively, these findings provide some understanding of the tissue-specific gene regulation mediated by ATF4 that could account for the divergent phenotypes in dividing fibroblasts versus postmitotic neurons.

Published May 5, 2008



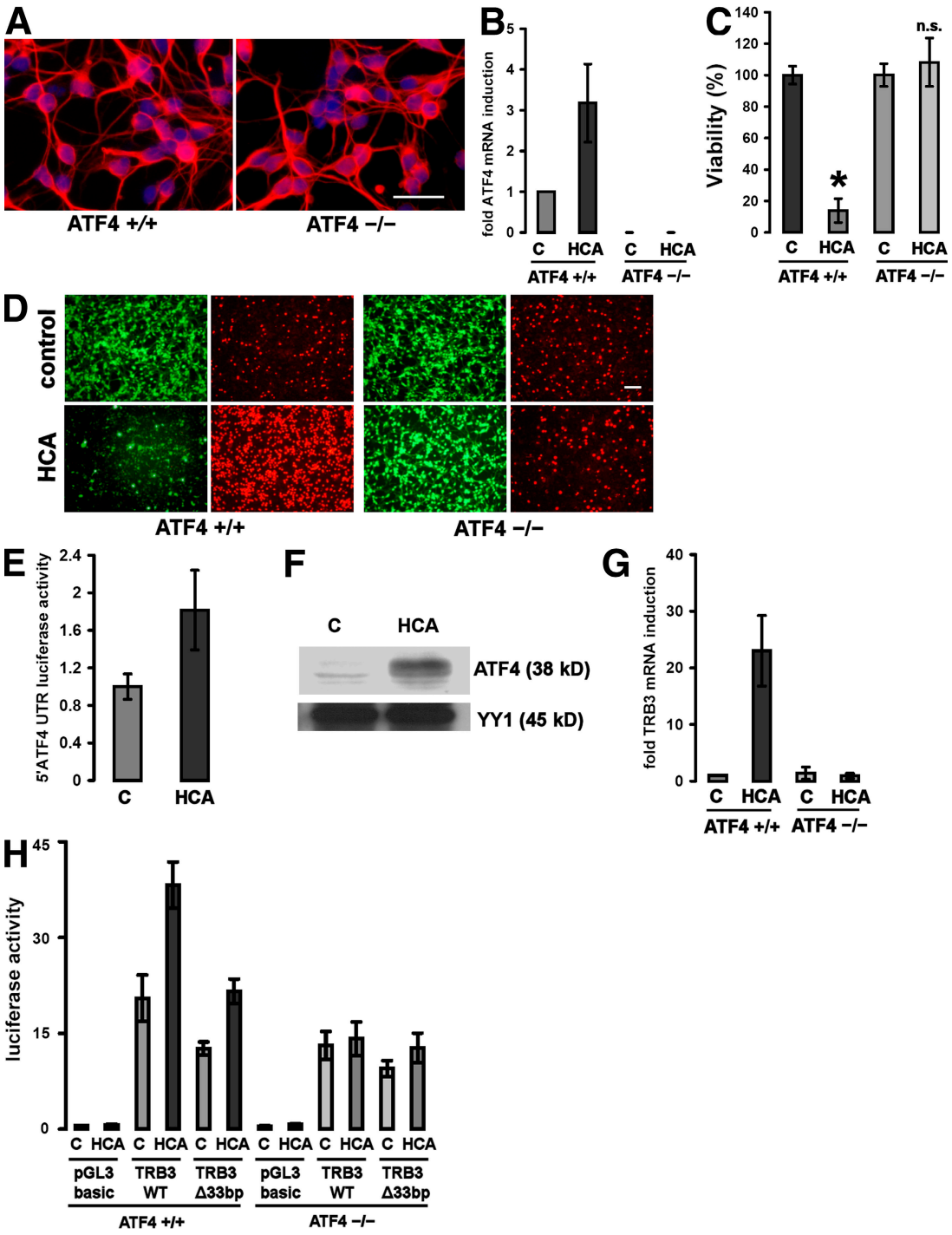


**Figure 2. Cortical neurons from ATF4$^{-/-}$ brains are resistant to oxidative stress–induced cell death.** (A) Immunocytochemistry of cultured ATF4$^{+/+}$ and ATF4$^{-/-}$ cortical neurons. Cells were stained with an antibody against MAP2 (which stains neural dendrites; red) and counterstained with Hoechst (blue). Bar, 50 µm. (B) Real-time PCR of ATF4 mRNA expression in ATF4$^{+/+}$ and ATF4$^{-/-}$ neurons in response to treatment with 10 mM HCA. The value obtained from the ATF4$^{+/+}$ control was arbitrarily defined as 1. Mean ± SD was calculated from three separate experiments. Each data point was performed in duplicate. (C) Cortical neuronal cultures (1 d in vitro) prepared from brains from ATF4$^{+/+}$ and ATF4$^{-/-}$ embryos were treated with a vehicle control (shown as C) or 10 mM HCA. 24 h later, cell viability was determined using the MTT assay. The graph depicts mean (compared with control) ± SD calculated from data from five separate experiments ($n$ = 27 ATF4$^{+/+}$ and 73 ATF4$^{-/-}$). *, P < 0.05 from ATF4$^{+/+}$ untreated cultures by the Kruskal-Wallis test followed by Dunn's multiple comparisons test. The difference between treated and untreated ATF4$^{-/-}$ neurons was not significant (n.s.). (D) Representative live/dead assay displaying untreated and HCA-treated ATF4$^{+/+}$ and ATF4$^{-/-}$ neurons. Bar, 50 µm. (E) ATF4$^{+/+}$ neurons were transfected with a reporter plasmid (pGL3 backbone) containing the mouse ATF4 5′UTR and AUG fused to luciferase. Cortical neurons were cotransfected with a plasmid expressing Renilla to allow normalization for transfection efficiency. 24 h after transfection, neurons were treated with vehicle control (shown as C) or 10 mM HCA. Cells were harvested in luciferase assay buffer 12 h after the onset of treatment. Values were

Published May 5, 2008



### Overexpression of ATF4 is sufficient to restore sensitivity to glutathione depletion–induced cell death and is capable of inducing cell death by itself

Because we used germline knockout animals (19) in this study, we could not exclude the possibility that the decreased susceptibility to oxidative stress was a consequence of a compensatory effect distantly related to ATF4 deficiency. To address this question, we used adenoviral overexpression of a mouse ATF4WT construct. As a control, we used a dominant-negative ATF4 construct harboring a mutation in its DNA binding domain ($^{292}$RYRQKKR$^{298}$ to $^{292}$GYLEAAA$^{298}$). To confirm the different DNA binding properties of these constructs, we analyzed the 33-bp binding region of the TRB3 promoter by gel-shift (Fig. 4 A) and chromatin immunoprecipitation studies (Fig. 4 B). In fact, only nuclear extracts from cells overexpressing ATF4WT in combination with WT oligonucleotide formed a band specific for ATF4. Consistently, only TRB3 promoter chromatin from cells overexpressing ATF4WT could be PCR amplified using primers flanking the ATF4 binding site. Cotransfection of WT and mutant ATF4 constructs with reporter constructs containing the WT and the mutant binding site confirmed the activating effect ATF4 has on transcription (Fig. 4 C).

To determine whether forced expression of ATF4 in ATF4$^{-/-}$ neuronal cultures can restore sensitivity to oxidative stress and/or has an effect itself, we overexpressed both constructs along with a GFP control in both ATF4$^{+/+}$ and ATF4$^{-/-}$ cortical neuronal cultures, followed by treatment with HCA (Fig. 5). We confirmed the efficient expression of both ATF4 constructs in cortical neurons by immunohistochemistry (Fig. 5 A) and Western blotting (Fig. 5 B). Specifically, ∼50% of neurons and a small number of glia are infected with the adenoviruses. Infection with ATF4ΔRK was able to protect ATF4$^{+/+}$ cortical neuronal cultures from HCA-induced toxicity (Fig. 5, C and D), whereas infection with ATF4WT was capable of rendering ATF4$^{-/-}$ neurons sensitive to HCA (Fig. 5, E and F). Moreover, infection with ATF4WT itself significantly reduced the viability in both WT and ATF4$^{-/-}$ neurons. Combination of forced expression of ATF4WT and treatment with HCA resulted in a higher loss of viability than infection with ATF4WT alone, suggesting that at least one more pathway in addition to ATF4 is involved in HCA toxicity. Collectively, these results are consistent with the notion that ATF4 indeed plays a key role in oxidative stress–mediated cell death.

### ATF4 has a negative impact on neuronal glutathione metabolism

The loss of glutathione is central to the in vitro model of oxidative stress used in this study. This model has been successfully used to describe signaling pathways that prevent cell death downstream of glutathione depletion. However, in fibroblasts, ATF4 has been described as a positive regulator of glutathione metabolism (11). Therefore, we performed glutathione measurements to determine whether ATF4 permits cell death in response to HCA by direct influence of the neuronal glutathione metabolism or by acting downstream of glutathione depletion. In untreated neurons, glutathione concentrations in ATF4$^{+/+}$ and ATF4$^{-/-}$ neurons did not differ (Fig. 6 A). As anticipated, HCA treatment caused a progressive loss of glutathione in ATF4$^{+/+}$ neurons. However, ATF4$^{-/-}$ neurons displayed a markedly slower decline in glutathione concentration. To rule out the possibility that an increased rate of glutathione synthesis is responsible for decreased sensitivity to cystine deprivation–induced glutathione depletion (20), we used buthionine sulfoximine (BSO) to directly inhibit the rate-limiting enzyme of glutathione synthesis, γ-glutamylcysteine synthetase (γ-GCS; Fig. 6 B). BSO resulted in cell death in ATF4$^{+/+}$ neurons, whereas ATF4$^{-/-}$ neurons were essentially resistant (Fig. 6, C and D). As expected from these results, γ-GCS expression did not differ between ATF4$^{+/+}$ and ATF4$^{-/-}$ neurons at the protein level and did not appear in the gene array (Fig. 6 E). Similar to HCA, BSO treatment led to a decline in the concentration of glutathione in ATF4$^{+/+}$ neurons, whereas ATF4$^{-/-}$ neurons displayed a distinctly slower reduction of glutathione (Fig. 6 F). These findings are consistent with the notion that the differences in reduction of glutathione after HCA or BSO is not attributable to changes in synthesis. To determine whether ATF4 directly regulates the neuronal glutathione content, we measured glutathione in neurons with forced expression of ATF4WT, ATF4ΔRK, and GFP (Fig. 6 G). Consistent with the finding that forced expression of ATF4WT can reduce neuronal viability, we found that this viability reduction correlates with a reduction in the neuronal glutathione content. Because cell death attributable to glutathione depletion can be completely blocked by a whole host of classical antioxidants, we combined forced expression of ATF4WT with butylated hydroxyanisol (BHA) treatment (Fig. 6, H and I). BHA is a well characterized

calculated from three separate experiments and are given as the ratio of luciferase and Renilla activities (mean ± SD; $n = 3$). The value for treatment with vehicle control was arbitrarily defined as 1. (F) Oxidative stress results in nuclear accumulation of ATF4 in cultured cortical neurons. 60 µg of nuclear extracts from cortical neurons treated with 10 mM HCA or vehicle control (shown as C) were separated using gel electrophoresis and immunodetected using an antibody against ATF4. YY1 was monitored as a loading control. (G) Real-time PCR of TRB3 mRNA expression in ATF4$^{+/+}$ and ATF4$^{-/-}$ neurons in response to treatment with 10 mM HCA. The value obtained from the ATF4$^{+/+}$ control was arbitrarily defined as 1. Mean ± SD was calculated from three separate experiments. Each data point was performed in duplicate. (H) ATF4$^{+/+}$ and ATF4$^{-/-}$ neurons were transfected with a luciferase reporter plasmid (pGL3 backbone) containing a 2-kb fragment of the mouse TRB3 promoter (TRB3WT), with a mutant version of this promoter lacking the 33-bp ATF4 binding site (TRB3Δ33bp) or with the empty vector (pGL3 basic). Cortical neurons were cotransfected with a plasmid expressing Renilla to allow normalization for transfection efficiency. 24 h after transfection, neurons were treated with vehicle control (shown as C) or 10 mM HCA. Cells were harvested in luciferase assay buffer 12 h after the onset of treatment. Values are given as the ratio of luciferase and Renilla activities (mean ± SD) and were calculated from three separate experiments. Each data point was performed in duplicate. Values are given as the ratio of luciferase and Renilla activities (mean ± SD; $n = 3$). The value for empty pGL3 was arbitrarily defined as 1.

Published May 5, 2008



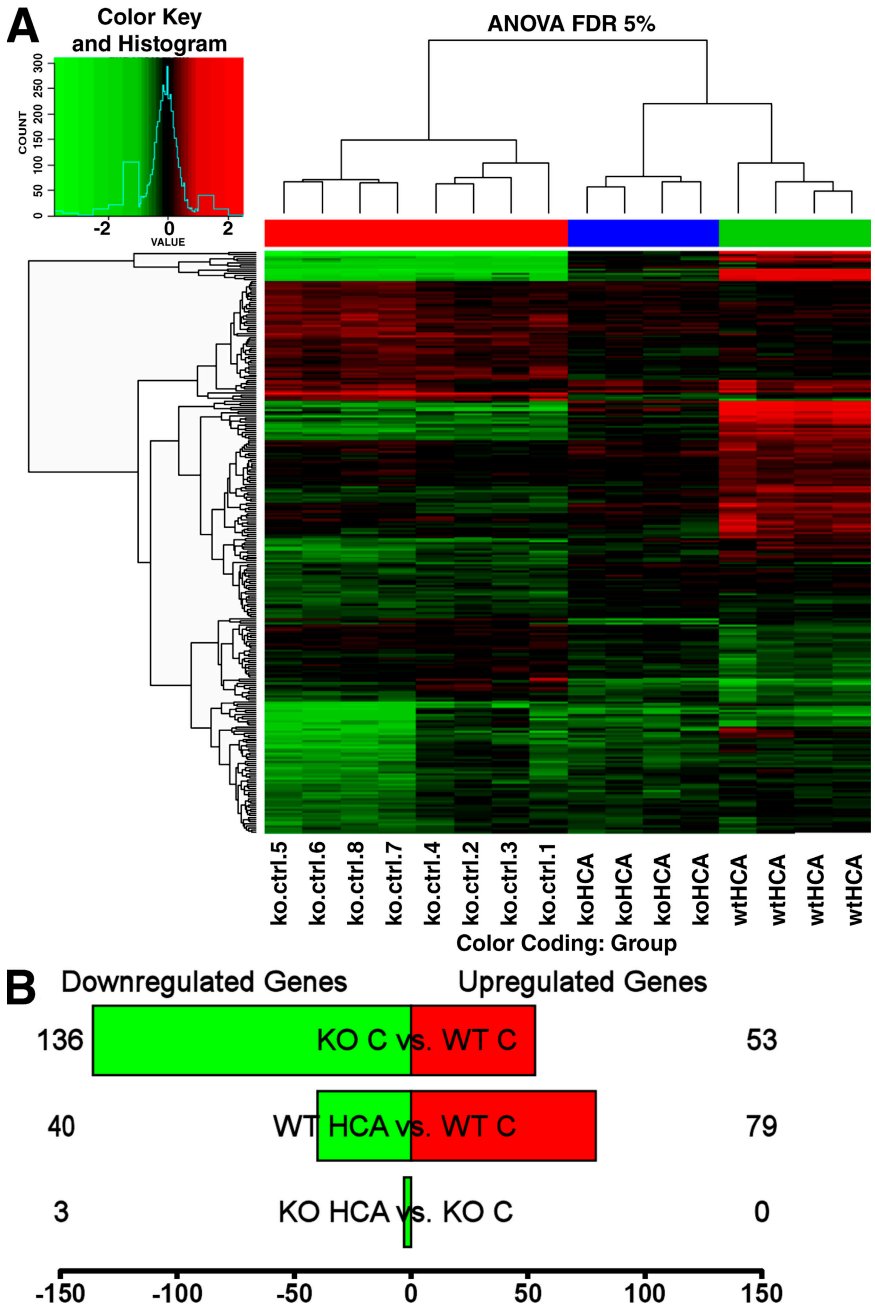


**Figure 3. Gene expression array analysis of ATF4$^{+/+}$ and ATF4$^{-/-}$ neurons before and after treatment with HCA.** (A) Heatmap with cluster dendrogram of the differentially expressed genes (log2 fold change vs. control) at a false discovery rate of 5%. Unsupervised clustering groups samples by genotype and by treatment. Genes are in rows and samples are in columns. Column color coding is as follows: red, ATF4$^{-/-}$ versus ATF4$^{+/+}$ untreated neurons; blue, HCA-treated ATF4$^{-/-}$ versus untreated ATF4$^{-/-}$ neurons; and green, HCA-treated ATF4$^{+/+}$ versus untreated ATF4$^{+/+}$ neurons. (B) The number of genes that are up- (red) and down-regulated (green). Shown are three different contrasts: ATF4$^{-/-}$ versus ATF4$^{+/+}$ untreated neurons, HCA-treated ATF4$^{+/+}$ versus untreated ATF4$^{+/+}$ neurons, and HCA-treated ATF4$^{-/-}$ versus untreated ATF4$^{-/-}$ neurons. The complete list of differentially expressed genes is available in Table S3 (available at http://www.jem.org/cgi/content/full/jem.20071460/DC1). ANOVA FDR, analysis of variance false discovery rate; C, control.

antioxidant known to block HCA-induced cell death in cortical neurons (6). In fact, in neurons overexpressing ATF4WT, BHA significantly increased neuronal viability and protected against the additional toxic effect of HCA treatment. Finally, we measured production of ROS by using the redox-sensitive probe 2′,7′-dichlorofluorescin (DCF; Fig. S1, available at http://www.jem.org/cgi/content/full/jem.20071460/DC1). Indeed, ATF4$^{-/-}$ neurons displayed lower levels of ROS in response to HCA treatment than ATF4$^{+/+}$ neurons. These findings are consistent with

Published May 5, 2008



**Table I.** Differentially expressed genes in ATF4$^{-/-}$ neurons versus ATF4$^{+/+}$ neurons before and after HCA treatment

| Symbol | Definition | KO.NTvsWT.NT | WT.HCAvsWT.NT | KO.HCAvsKO.NT |
|---|---|---|---|---|
| Atf4 | activating transcription factor 4 (Atf4) | -3.602 | 1.054 | -0.12 |
| Atf4 | activating transcription factor 4 (Atf4) | -3.342 | 0.507 | -0.148 |
| Slc7a3 | solute carrier family 7, member 3 (Slc7a3) | -2.185 | 0.973 | 0.085 |
| 1810008K03Rik | RIKEN cDNA 1810008K03 gene (1810008K03Rik) | -2.135 | 1.514 | -0.46 |
| Cox6a2 | cytochrome c oxidase, subunit VI a, polypeptide 2 (Cox6a2) | -1.63 | 0.008 | -0.046 |
| Eif4ebp1 | eukaryotic translation initiation factor 4E binding protein 1 (Eif4ebp1) | -1.479 | 1.366 | -0.593 |
| Slc7a5 | solute carrier family 7, member 5 (Slc7a5) | -1.414 | 1.035 | -0.324 |
| Mgat3 | mannoside acetylglucosaminyltransferase 3 (Mgat3) | -1.294 | 0.097 | 0.152 |
| Slc25a17 | solute carrier family 25, member 17 (Slc25a17) | 1.286 | 0.086 | -0.13 |
| Serpinf1 | serine (or cysteine) proteinase inhibitor, member 1 (Serpinf1) | -1.158 | 0.48 | -0.142 |
| 2510038A11Rik | RIKEN cDNA 2510038A11 gene (2510038A11Rik) | -1.153 | -0.255 | 0.215 |
| Slc6a9 | solute carrier family 6, member 9 (Slc6a9) | -1.138 | 1.045 | -0.235 |
| Atf5 | activating transcription factor 5 (Atf5) | -1.107 | 0.482 | -0.085 |
| Spon2 | spondin 2, extracellular matrix protein (Spon2) | -1.052 | -0.537 | -0.456 |
| Psat1 | phosphoserine aminotransferase 1 (Psat1) | -1.036 | 0.86 | -0.436 |
| Asns | asparagine synthetase (Asns) | -0.995 | 0.894 | -0.095 |
| Tgfbi | transforming growth factor, beta induced (Tgfbi) | -0.987 | -0.064 | -0.438 |
| Cars | cysteinyl-tRNA synthetase (Cars) | -0.947 | 1.614 | 0.254 |
| BC025519 | cDNA sequence BC025519 (BC025519) | -0.908 | -0.296 | -0.149 |
| Loxl1 | lysyl oxidase-like 1 (Loxl1) | -0.87 | -0.533 | -0.813 |
| Hes5 | hairy and enhancer of split 5 (Drosophila) (Hes5) | -0.838 | -0.754 | -0.149 |
| Mt3 | metallothionein 3 (Mt3) | -0.792 | -0.403 | -0.508 |
| Psat1 | phosphoserine aminotransferase 1 (Psat1) | -0.786 | 1.422 | 0.303 |
| Aqp4 | aquaporin 4 (Aqp4) | -0.778 | 0.173 | -0.163 |
| Mmp2 | matrix metalloproteinase 2 (Mmp2) | -0.754 | 0.195 | -0.41 |
| Trib3 | Tribbles homolog 3 (Trib3) | -0.75 | 1.613 | 0.017 |
| Scd1 | stearoyl-Coenzyme A desaturase 1 (Scd1) | -0.743 | 0.198 | -0.409 |
| Stard4 | StAR-related lipid transfer (START) domain containing 4 (Stard4) | -0.728 | 0.476 | -0.131 |
| Mthfd2 | methylenetetrahydrofolate dehydrogenase (Mthfd2) | -0.71 | 0.998 | -0.359 |
| Shmt2 | serine hydroxymethyl transferase 2 (mitochondrial) (Shmt2) | -0.709 | 0.653 | -0.051 |
| Egr1 | early growth response 1 (Egr1) | -0.704 | 0.07 | -0.387 |
| Nupr1 | nuclear protein 1 (Nupr1) | -0.7 | 1.549 | -0.224 |
| Slc3a2 | solute carrier family 3, member 2 (Slc3a2) | -0.656 | 0.825 | -0.002 |
| Sox21 | SRY-box containing gene 21 (Sox21) | -0.627 | -0.814 | -0.637 |
| Aars | alanyl-tRNA synthetase (Aars) | -0.616 | 0.568 | -0.058 |
| Nars | asparaginyl-tRNA synthetase (Nars) | -0.569 | 0.488 | -0.177 |
| Zfp312 | zinc finger protein 312 (Zfp312) | 0.54 | -0.736 | -0.3 |
| Fthfsdc1 | formyltetrahydrofolate synthetase domain containing 1 (Fthfsdc1) | -0.529 | 0.803 | -0.175 |
| Nrarp | Notch-regulated ankyrin repeat protein (Nrarp) | -0.52 | -0.679 | -0.493 |
| Vegfa | vascular endothelial growth factor A (Vegfa) | -0.505 | 1.254 | 0.016 |
| Hmox1 | heme oxygenase (decycling) 1 (Hmox1) | -0.498 | 1.843 | 0.504 |
| Ovgp1 | oviductal glycoprotein 1 (Ovgp1) | 0.459 | 0.658 | 0.498 |
| Asns | asparagine synthetase (Asns) | -0.458 | 0.902 | 0.072 |
| Slc1a4 | solute carrier family 1, member 4 (Slc1a4) | -0.456 | 0.843 | 0.072 |
| D330038I09Rik | RIKEN cDNA D330038I09 gene (D330038I09Rik) | -0.323 | 0.669 | 0.094 |
| Mt1 | metallothionein 1 (Mt1) | -0.275 | -0.115 | -0.711 |
| Fosb | FBJ osteosarcoma oncogene B (Fosb) | 0.239 | -0.161 | -0.886 |
| Ddit4 | DNA-damage-inducible transcript 4 (Ddit4) | -0.211 | 1.043 | -0.017 |
| Aard | alanine and arginine rich domain containing protein (Aard) | -0.174 | -0.869 | -0.516 |
| Vldlr | very low density lipoprotein receptor (Vldlr) | -0.149 | 0.74 | 0.306 |
| Tars | threonyl-tRNA synthetase (Tars) | -0.146 | 0.759 | 0.261 |
| Sv2b | synaptic vesicle glycoprotein 2 b (Sv2b) | 0.139 | -0.858 | -0.709 |
| Plat | plasminogen activator, tissue (Plat) | -0.06 | -0.131 | -0.42 |
| Cyp26b1 | cytochrome P450, family 26b, polypeptide 1 (Cyp26b1) | 0.007 | -0.803 | -0.541 |

From each of the three contrasts, the top 30 genes with the highest fold change were selected. Ratios are log2 transformed. Up-regulated genes (fold change > 0.2) are highlighted in red, and down-regulated genes (fold change < −0.2) are highlighted in green.

the notion that ATF4 positively influences ROS levels and leads to a higher consumption of glutathione independent of its synthesis.

### ATF4$^{-/-}$ animals are less susceptible to ischemic brain damage

Oxidative stress is an established mediator of neuronal loss in cerebral ischemia (21). It is generally accepted that glutathione acts as a major endogenous cerebral antioxidant in the adult brain. In fact, depletion of intracellular antioxidants has been associated with stroke pathology and repletion of antioxidants has reduced neuronal damage (22). Therefore, we hypothesized that ATF4 deficiency might positively influence the antioxidant status in the adult brain and thereby improve the outcome after ischemia-reperfusion injury. To test the hypothesis that ATF4 germline knockout animals have less neuronal loss after stroke, we used a transient middle cerebral artery occlusion (MCAo) model for ischemia-reperfusion injury, as previously described (23).

Published May 5, 2008



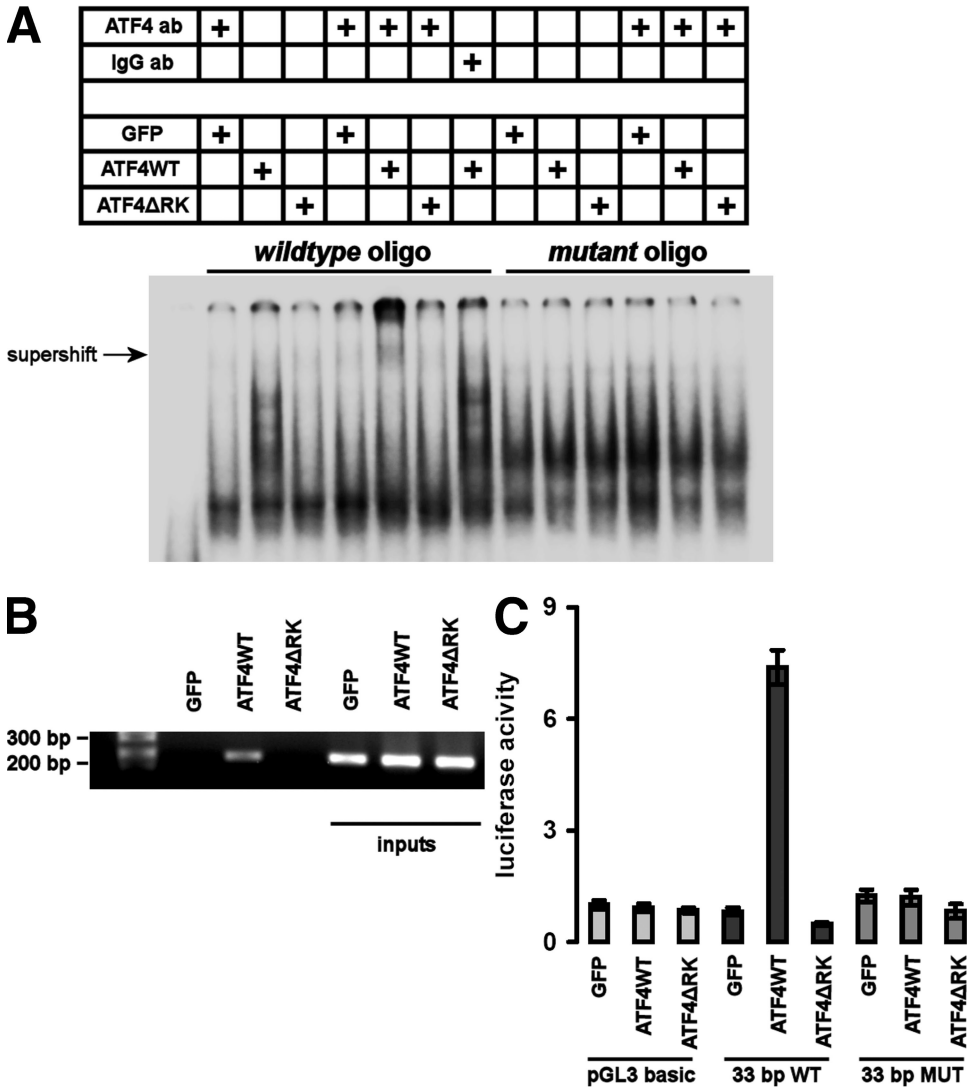


**Figure 4. ATF4 binds to a 33-bp binding element within the TRB3 promoter.** (A) EMSA performed with 10 µg of dialyzed nuclear extracts from HT22 cells transfected with ATF4WT, mutant ATF4 (ATF4ΔRK), or GFP, respectively. Extracts were incubated with a radioactively labeled WT oligonucleotide containing the TRB3 promoter binding site or with a mutant oligonucleotide. Binding of ATF4WT to the TRB3WT promoter binding site was confirmed by supershift analysis (arrow) performed with an antibody (Ab) directed against ATF4. (B) Overexpressed ATF4WT protein occupies its putative binding site within the TRB3 promoter in HT22 cells, as shown by chromatin immunoprecipitation assay. HT22 cells were transfected with ATF4WT, mutant ATF4 (ATF4ΔRK), or GFP. An anti-myc antibody was used to precipitate the proteins in nuclear extracts of cross-linked HT22 cells. Coprecipitated DNA fragments were detected using PCR with a set of primers specific for the ATF4 binding site in the TRB3 promoter, yielding a 190-bp product. A representative example of three experiments is shown. (C) HT22 cells were transfected with the expression plasmids for ATF4WT, mutant ATF4 (ATF4ΔRK), or GFP. The cells were cotransfected with either a luciferase reporter vector containing the 33-bp ATF4WT binding site (33 bp WT), a reporter vector containing a mutant form of this binding site (33 bp MUT), or empty vector (pGL3 basic). In parallel, the transfection mix contained a plasmid expressing Renilla to allow normalization for transfection efficiency. The value for empty pGL3 cotransfected with GFP was arbitrarily defined as 1. Shown are ratios of luciferase and Renilla activities (mean ± SD for three independent experiments; each data point was performed in duplicate).

First, we performed morphological studies to rule out that germline ATF4 deficiency causes a fundamental abnormality in the adult brain that would bias stroke outcome (19, 24–26). Examining sagittal sections of brains from $ATF4^{+/+}$ and $ATF4^{-/-}$animals (Fig. 7 A, top), we did not detect any significant structural differences in the cerebellum, hippocampus, or cortex. We then assessed the morphology of major cerebral blood vessels of the circle of Willis (Fig. 7 A, middle) (23). Besides a higher degree of tortuosity in the MCA, no major abnormalities were detected in the brains obtained from $ATF4^{-/-}$ mice. Finally, using immunofluorescent staining for the endothelial-specific marker CD31/PECAM, we did not observe significant differences in the density or morphology of the microvessels (Fig. 7 A, bottom). In addition, important

Published May 5, 2008



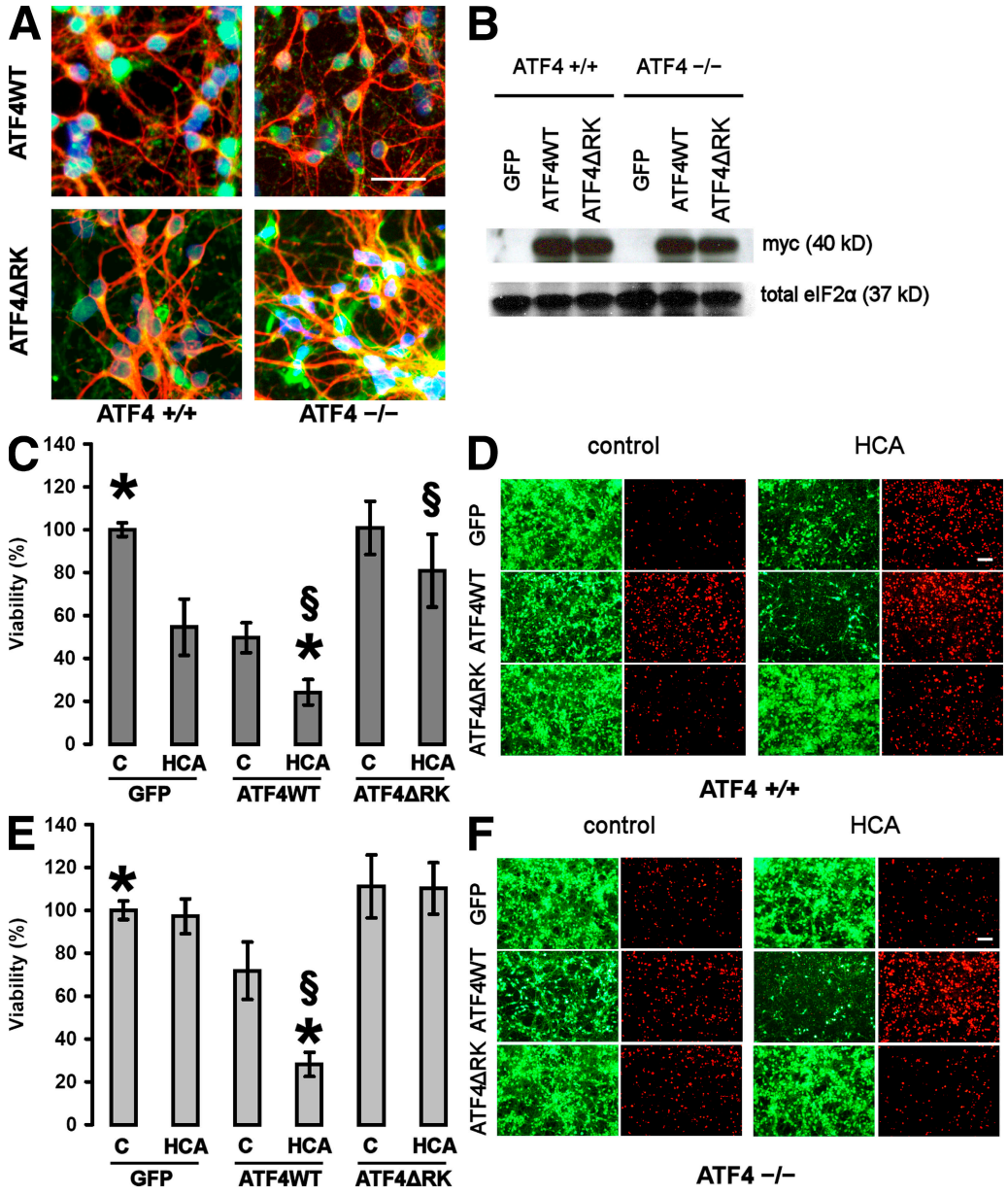


**Figure 5. Overexpression of ATF4WT restores sensitivity to oxidative stress and reduces neuronal viability itself.** (A) Representative immunocytochemistry of ATF4$^{+/+}$ and ATF4$^{-/-}$ cortical neurons infected with the adenoviral constructs ATF4WT and ATF4ΔRK. Neurons were stained with antibodies against myc (green) and MAP2 (red), and were counterstained with Hoechst dye (blue). Bar, 50 µm. (B) Whole-cell extracts obtained from both ATF4$^{+/+}$ and ATF4$^{-/-}$ neurons infected with GFP, ATF4WT, and ATF4ΔRK were separated using gel electrophoresis and immunodetected using an antibody directed against the myc tag. Total eIF2α was monitored as a loading control. (C) ATF4$^{+/+}$ cortical neurons were infected with GFP, ATF4WT, and ATF4ΔRK adenoviruses at an MOI of 100. 24 h after infection, neurons were treated with vehicle control (shown as C) or 10 mM HCA. 24 h later, cell viability was determined using the MTT assay. The graph depicts mean (compared with control) ± SD calculated from four separate experiments for each group ($n$ = 45). $P < 0.05$ by the Kruskal-Wallis test followed by Dunn's multiple comparisons test from untreated ATF4WT-overexpressing neurons (*) and from HCA-treated neurons overexpressing GFP (§). (D) Live/dead assay. Bar, 50 µm. (E) ATF4$^{-/-}$ cortical neurons were infected with GFP, ATF4WT, and ATF4ΔRK adenoviruses at an MOI of 100. 24 h after infection, neurons were treated with vehicle control (shown as C) or 10 mM HCA. 24 h later, cell viability was determined using the MTT assay. The graph depicts mean (compared with control) ± SD calculated from four separate experiments for each group ($n$ = 28). $P < 0.05$ by the Kruskal-Wallis test followed by Dunn's multiple comparisons test from untreated ATF4WT-overexpressing neurons (*) and from HCA-treated neurons overexpressing GFP (§). (F) Live/dead assay. Bar, 50 µm.

physiological parameters did not differ between ATF4$^{+/+}$ and ATF4$^{-/-}$ animals (Fig. S2 and Table S2, available at http://www.jem.org/cgi/content/full/jem.20071460/DC1).

The procedure used to occlude the MCA (occlusion time = 45 min) led to reproducible infarcts in WT animals involving both the cerebral cortex and the striatum, with sparing of

Published May 5, 2008



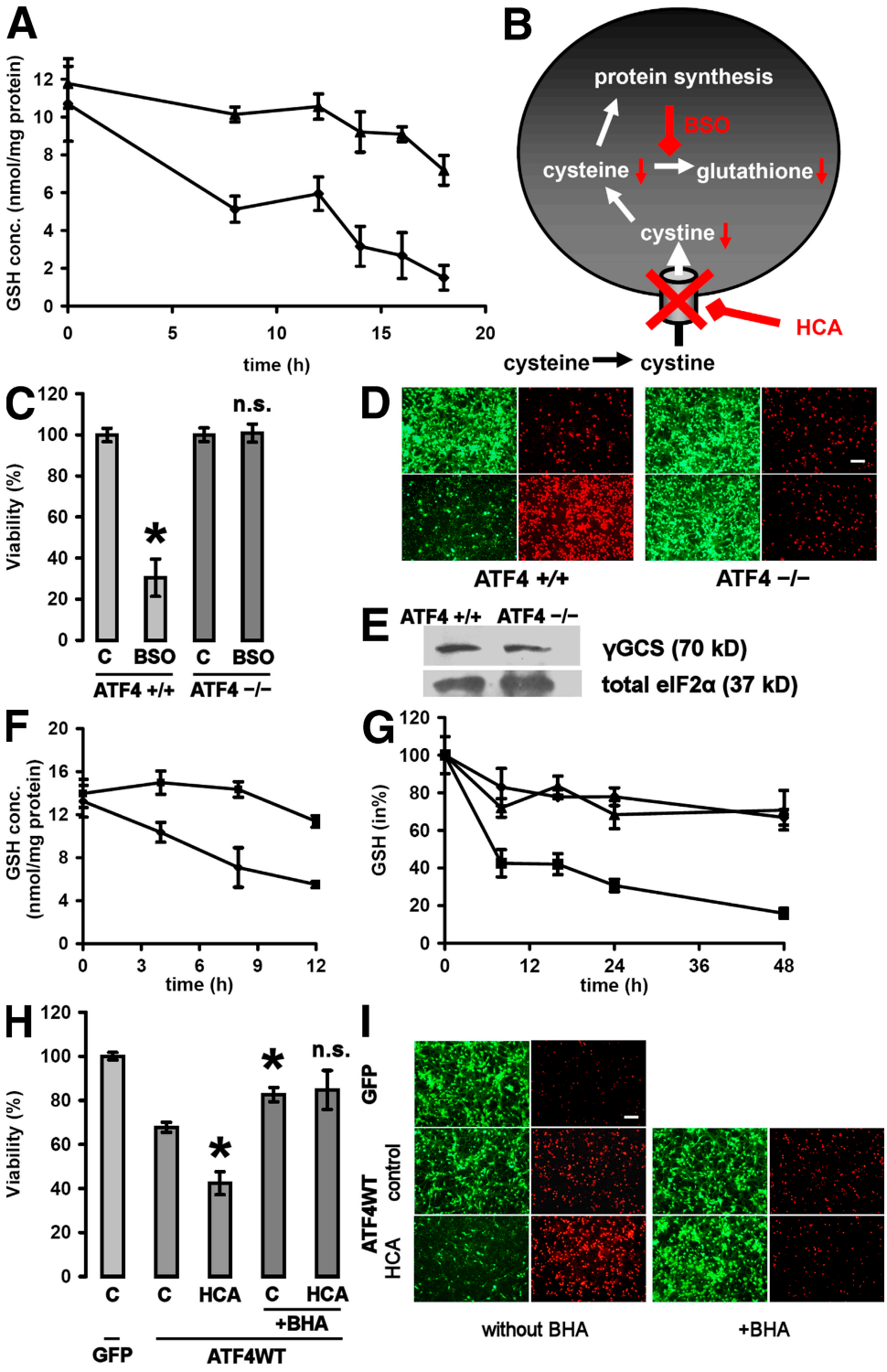


**Figure 6. ATF4 has a negative impact on the neuronal glutathione metabolism.** (A) ATF4$^{+/+}$ (◆) and ATF4$^{-/-}$ (▲) cortical neurons were treated with 10 mM HCA. At the indicated time points, cells were trypsinized, washed, and pelleted. Reduced glutathione (GSH) was determined in the cell pellets using HPLC electrochemical detection. Data are from three separate cultures, and each data point was measured in duplicate. Graph depicts mean ± SD. (B) Schematic overview over cysteine uptake and glutathione synthesis and their inhibition. (C) ATF4$^{+/+}$ and ATF4$^{-/-}$ cortical neurons were treated with a vehicle control (shown as C) or 200 µM BSO. 24 h later, cell viability was determined using the MTT assay. The graph depicts mean (compared with control) ± SD calculated from five separate experiments for each group ($n$ = 46 ATF4$^{+/+}$ and 58 ATF4$^{-/-}$). *, $P < 0.05$ from untreated ATF4$^{+/+}$ cultures by the Kruskal-Wallis test followed by Dunn's multiple comparisons test. The difference between treated and untreated ATF4$^{-/-}$ neurons was not significant (n.s.). (D) Live/dead assay displaying untreated and BSO-treated ATF4$^{+/+}$ and ATF4$^{-/-}$ neurons. Bar, 50 µm. (E) Protein expression of γ-GCS does not differ between ATF4$^{+/+}$ and ATF4$^{-/-}$ cortical

Published May 5, 2008



the hippocampus. However, a significantly smaller infarct was observed when the procedure was performed in ATF4$^{-/-}$ animals (Fig. 7, C and D). The smaller infarct area could be observed in all sections of the brain. Thus, the higher resistance to ischemia-reperfusion injury was not limited to a specific brain area. In fact, the smaller infarct volume was associated with a faster recovery in ATF4$^{-/-}$ animals, as measured by a simple neurological score (Fig. 7 E). In addition, two simple behavioral tests (Fig. 7, F and G) complemented the morphological data. In consideration of the eye lens malformation regularly observed in ATF4$^{-/-}$ animals (25), these tests are not dependent on the visual sense. Consistent with the morphological data, ATF4$^{-/-}$ animals performed significantly better than the ATF4$^{+/+}$ control group, suggesting that ATF4 deficiency facilitates recovery after stroke.

## DISCUSSION

### ATF4 is a prodeath transcription factor

Solid evidence supports the hypothesis that oxidative stress is an initiator or propagator of neuronal dysfunction or death in prevalent neurological diseases, including stroke, spinal cord injury, Alzheimer's disease, and Parkinson's disease (3, 27). These studies have led to the somewhat surprising conclusion that oxidants can trigger neuronal death via highly regulated signaling pathways and subsequent activation of prodeath transcription factors, leading to the controlled demise known as apoptosis (28). The current study adds to our understanding of the cellular transcription factors that regulate neuronal viability and function after oxidative stress in primary cortical neurons. Specifically, we show that the transcription factor ATF4 is induced by oxidative stress caused by depletion of the major antioxidant tripeptide, glutathione. We further demonstrate that transgenic deletion of ATF4 renders neurons resistant to neuronal cell death. Prevention of cell death by germline knockout of ATF4 is associated with a preservation of glutathione levels, the primary mediator of death in our oxidative stress model. Consistent with ATF4's role in regulating an early, upstream aspect of the oxidative neuronal death pathway, we found that ATF4 deficiency causes global down-regulation of gene expression and blocks the up-regulation of many genes that are induced by oxidative stress in WT neurons. Accordingly, forced expression of ATF4 was sufficient to promote cell death and loss of glutathione. In addition, we demonstrate that in ATF4$^{-/-}$ neurons, restoration of ATF4 protein expression reinstated sensitivity to oxidative death. We establish the relevance of protection by ATF4 deficiency by demonstrating that the ATF4 homozygous knockout is capable of protecting the adult mouse brain from stroke-induced injury and disability. Indeed, we show that ATF4$^{-/-}$ animals recover more easily and maintain proper motor function more efficiently. Although known to be a stress-responsive protein, these results for the first time establish ATF4 as a redox-regulated protein that can function to lower the threshold for oxidative stress–induced death in neurons.

### ATF4 is a redox-regulated transcription factor

Classically, stress-mediated enhancement of ATF4 levels is known to occur via enhanced efficiency of translation of constant levels of ATF4 mRNA (29, 30). Consistent with this model, we found an up-regulation of ATF4 mRNA translational efficiency after glutathione depletion. However, we also observed an increase in ATF4 mRNA levels after oxidative stress, thereby confirming a recent report describing a role for transcriptional regulation in ATF4 induction by cell stress (31). The distinct increase in ATF4 protein levels in the nucleus of neurons undergoing oxidative stress corresponded to an ATF4-dependent induction of a TRB3 promoter-luciferase reporter. Collectively, these observations argue that oxidative stress–induced changes in ATF4 mRNA levels and translational efficiency lead to increased ATF4 activity in neurons. Because ATF4 overexpression is sufficient to induce death, limiting the amount of ATF4, at least under basal conditions, seems to be necessary for neuronal survival. Mechanisms that control and limit basal ATF4 activity (32–34) appear to be important determinants of neuronal fate. Although this low level of ATF4 appears to be sufficient to regulate a host of genes, its absence does not grossly influence neuronal morphology or basal survival.

### ATF4 has a direct impact on glutathione metabolism

Several converging lines of inquiry demonstrate a central role for glutathione metabolism in degeneration and aging in the nervous system. Our findings confirm the primary role that glutathione can play in neuronal death. However, the mechanisms by which a global depletion of glutathione in neurons is transduced into apoptotic events remained elusive. The data presented in this study favor a model in

neurons. Cytoplasmic extracts were separated using gel electrophoresis and immunodetected using an antibody against γ-GCS. Total eIF2α was monitored as a loading control. (F) ATF4$^{+/+}$ (◆) and ATF4$^{-/-}$ (■) cortical neurons were treated with 200 μM BSO. At the indicated time points, cells were trypsinized, washed, and pelleted. GSH was determined in the cell pellets using HPLC electrochemical detection. Data are from three separate cultures, and each data point was measured in duplicate. Graph depicts mean ± SD. (G) ATF4$^{+/+}$ cortical neurons were infected with GFP (◆), ATF4WT (■), and ATF4ΔRK (▲) adenoviruses at an MOI of 100. At the indicated time points after infection, cells were trypsinized, washed, and pelleted. GSH was determined in the cell pellets using HPLC electrochemical detection. The graph depicts mean ± SD calculated from three separate experiments for each group, and each data point was measured in duplicate. The value obtained from noninfected neurons was arbitrarily defined as 100%. (H) ATF4$^{+/+}$ cortical neurons were infected with GFP and ATF4WT adenoviruses at an MOI of 100. 24 h after infection, neurons were treated with vehicle control (shown as C), 10 mM HCA, 10 μM BHA, or a combination of both. The graph depicts mean (compared with control) ± SD calculated from five separate experiments for each group ($n$ = 29). *, $P < 0.05$ from untreated neurons overexpressing ATF4WT by the Kruskal-Wallis test followed by Dunn's multiple comparisons test. The difference between neurons overexpressing ATF4WT treated with BHA alone and neurons overexpressing ATF4WT treated with both BHA and HCA was not significant (n.s.). (I) Live/dead assay. Bar, 50 μm.

Published May 5, 2008



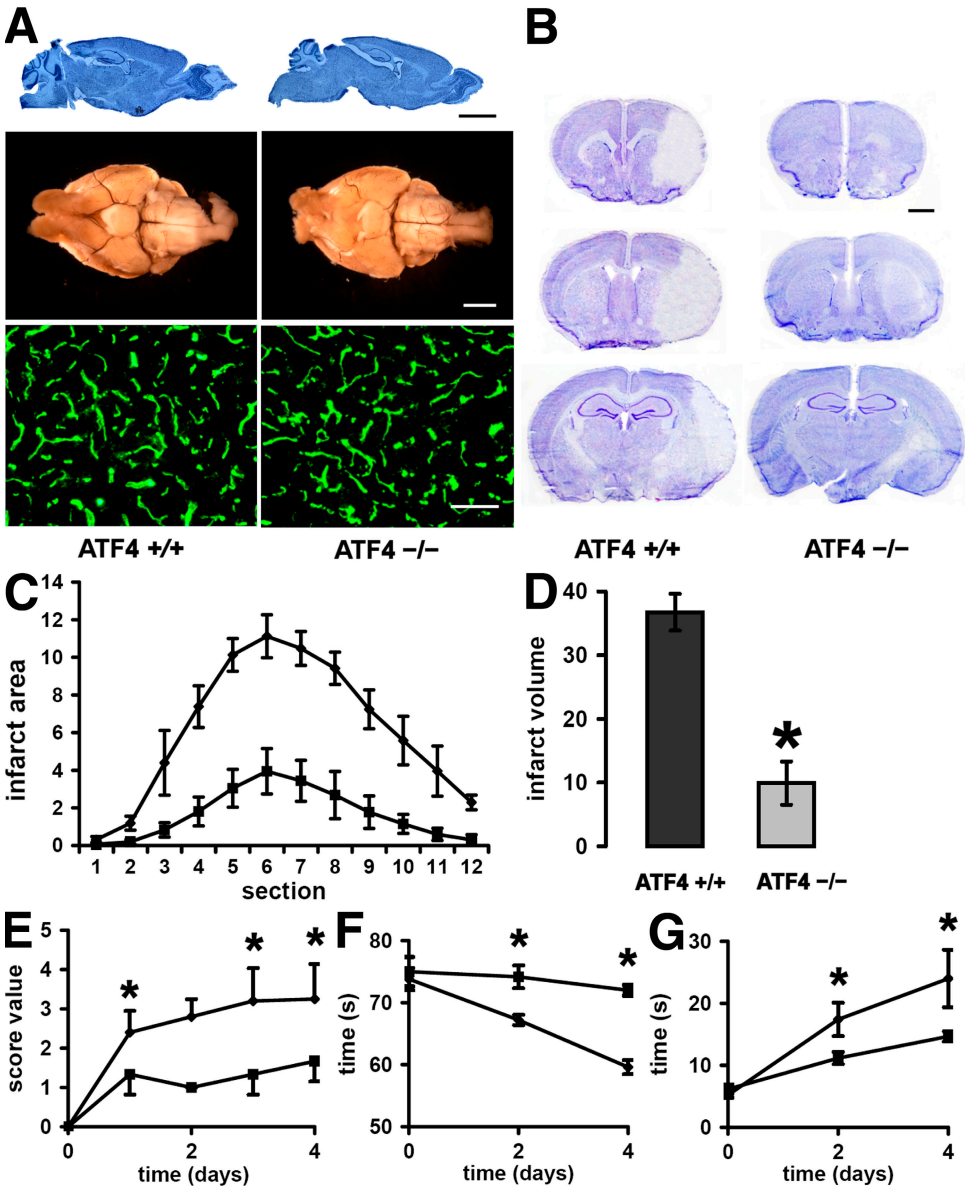


**Figure 7. Role of ATF4 in brain ischemia.** (A, top) Sagittal sections of ATF4$^{+/+}$ (left) and ATF4$^{-/-}$ (right) brains stained with cresyl violet. Bar, 3,000 µm. (A, middle) Ventral view of large cerebral blood vessels of representative ATF4$^{+/+}$ (left) and ATF4$^{-/-}$ (right) mice that were perfused with India ink. Note the higher degree of tortuosity of the MCA in the brain from the ATF4$^{-/-}$ mouse. Bar, 3,000 µm. (A, bottom) Representative microscopic views of brain sections from ATF4$^{+/+}$ and ATF4$^{-/-}$ mice that were immunostained for the endothelial cell–specific marker CD31 (green). Bar, 100 µm. (B) Representative brain sections at 4 d after MCAo from ATF4$^{+/+}$ ($n = 5$) and ATF4$^{-/-}$ ($n = 6$) mice from rostral to caudal stained with cresyl violet to determine the infarct area. Bar, 1,000 µm. (C) The infarct area in ATF4$^{+/+}$ (◆) and ATF4$^{-/-}$ (■) brains was measured in 12 sequential sections taken from ATF4$^{+/+}$ ($n = 5$) and ATF4$^{-/-}$ ($n = 6$) mice at rostral to caudal regular intervals. Graph depicts mean ± SD. (D) The infarct volume was assessed by adding the infarct volumes based on the infarct area in each section. Graph depicts mean ± SD. *, $P < 0.0001$ by the *t* test. (E) Scoring of neurological deficit was assessed at different time points of recovery in ATF4$^{+/+}$ ($n = 5$) and ATF4$^{-/-}$ ($n = 4$) mice. Graph depicts mean ± SD. *, $P < 0.05$ by the Mann-Whitney test. (F) Inclined plane test at different time points after stroke in ATF4$^{+/+}$ ($n = 5$) and ATF4$^{-/-}$ ($n = 4$) mice. The test measured the time a mouse managed to hold itself on an inclined glass plate angled at 50° before sliding down. Graph depicts mean ± SD. *, $P < 0.05$ by the *t* test. (G) Hanging wire test at different time points after stroke in ATF4$^{+/+}$ ($n = 5$) and ATF4$^{-/-}$ ($n = 4$) mice. The hanging wire test determined the time it took an animal to cross a distance of 45 cm on a freely hanging narrow metal bar. Graph depicts mean ± SD. *, $P < 0.05$ by the *t* test.

which glutathione depletion causes an ATF4-dependent up-regulation of a coordinated set of genes that orchestrate the timely and irreversible demise of the cell. Part of the orchestrated sequence of events downstream of ATF4 activation includes the increased production of ROS and turnover of glutathione. Although our data clearly establish that ATF4 induction does not influence glutathione synthesis, we cannot determine whether the increased turnover of

Published May 5, 2008



glutathione is primarily attributable to a change in a glutathione-degrading enzyme with a subsequent increase of ROS, or a secondary consequence of ATF4-mediated ROS production. Increased ROS production would be expected to decrease glutathione levels by enzyme-mediated consumption of the thiol tripeptide. Of note, many mitochondrial genes that could facilitate production of deleterious ROS during respiration are down-regulated in the $ATF4^{-/-}$ neurons. Future studies will clarify whether ATF4 mediates death primarily by altering glutathione turnover or by dialing up the production of free radicals.

### ATF4 induces global transcriptional changes

ATF4 was originally described as a transcriptional repressor (35, 36). However, our gene array data suggest that ATF4 acts at least in part as a transcriptional activator. This finding is in line with several more recent publications that describe the activating effect of ATF4 on several target genes, such as heme oxygenase 1 (37, 38), stanniocalcin 2 (39), osteocalcin (40), gadd153/CHOP (41), and TRB3 (42). Some of these target genes have been shown to play an important role in cell death and cell survival in the brain. Pharmacological induction of heme oxygenase 1 was demonstrated to protect neurons from oxidative insults both in vitro and in vivo (43). Indeed, heme oxygenase 1 is induced in WT neurons by oxidative stress; however, it was down-regulated in $ATF4^{-/-}$ neurons. Likewise, stanniocalcin 2 is up-regulated in response to oxidative stress in WT neurons but was down-regulated in $ATF4^{-/-}$ neurons. In a recent work (39), stanniocalcin 2 was identified as an oxidative stress–responsive gene with cytoprotective properties. A prodeath ATF4 target gene, TRB3, was strongly dependent on ATF4 and up-regulated in response to oxidative stress. TRB3's role in neuronal apoptosis was described first in a neuronal cell line (44) and has been recently confirmed (42).

### The prodeath role of ATF4 might be context and cell type specific

The data presented in this work are in support of a strong prodeath role of ATF4. However, previous findings regarding the roles of ATF4 have yielded partly different results. $ATF4^{-/-}$ fibroblasts are impaired in expressing genes involved in amino acid import, glutathione biosynthesis, and resistance to oxidative stress (11). Therefore, ATF4 was proposed to play a key role in rendering the cell more resistant against the metabolic consequences of endoplasmic reticulum oxidation. Therefore, we initially hypothesized that ATF4 induction by endoplasmic reticulum stress or amino acid depletion is the key event in the protection against oxidative stress mediated by HCA treatment (Fig. 1). The finding that ATF4 activation can be associated with protection from oxidative stress–induced cell death, although it clearly acts as a prodeath transcription factor, points to a complex and context-specific role of ATF4 in the propagation of neuronal cell death. However, both endoplasmic reticulum stress or amino acid depletion initiate several different signaling events in addition to ATF4 induction (2, 45). Which of these signaling events are capable of preventing the deleterious consequences of ATF4 activation requires further investigation. In general, the similarity of data obtained from fibroblasts and from cortical neurons is limited. However, despite the opposite effects on glutathione metabolism and cell survival, a comparison between the array data from fibroblasts with our gene expression data indicates a highly significant overlap. Even though the role of each of the many target genes of ATF4 warrant further investigation, the different metabolic demands of postmitotic neurons and actively dividing fibroblasts might help to explain the distinct role of ATF4 in distinct cell types (46). Additionally, differently expressed dimerization partners of ATF4 might also significantly modify ATF4's function. Indeed, several different cancer cell lines show an elevated level of ATF4 expression (10, 47–50). Moreover, ATF4 is already known to have functions that are limited to a specific cell type such as osteoblasts (40, 51, 52). The precise characterization of these additional signaling events warrants further investigation, and might help to explain why and how these signaling events are capable of preventing the deleterious consequences of ATF4 induction.

### ATF4 is a prodeath transcription factor in vivo

We have established that ATF4 also plays an important prodeath role in an in vivo model of stroke. However, the use of conventional $ATF4^{-/-}$ animals poses a risk of bias on the outcome in a complex paradigm such as stroke (53). Therefore, the results need to be interpreted with caution. We cannot rule out the possibility that ATF4 deficiency in all cell types of the brain and the body has an impact on stroke outcome. However, no overt difference was observed when comparing the brain morphology between WT and $ATF4^{-/-}$ brains, including the vascular system. In addition, the smaller infarct size in the $ATF4^{-/-}$ mice could not be attributed to changes in systemic physiological parameters, including body temperature, or changes in cerebral blood flow under basal conditions or after MCAo. However, an issue that was not addressed in this study is whether the $ATF4^{-/-}$ mice displayed an altered inflammatory response after ischemia that could explain the smaller infarct size. Although a higher propensity to infections or other immune-related alterations has not yet been observed in $ATF4^{-/-}$ mice, we cannot rule out the possibility that an altered inflammatory response (54) is one reason for the smaller infarct volume in the $ATF4^{-/-}$ mice. In summary, the strong correlation in the outcome between in vitro and in vivo studies lets us conclude that our results, even when reviewed carefully, suggest an important role for ATF4 in the induction of neuronal cell death. Thus, ATF4 might be an important target for therapeutic intervention against stroke and other neurodegenerative diseases.

## MATERIALS AND METHODS

**Animals.** All animal procedures were performed according to protocols approved by the Institutional Animal Care and Use Committee of the Weill Medical College of Cornell University. Germline $ATF4^{-/-}$ mice have been described previously (19). For the culture of mouse embryonic cortical

Published May 5, 2008



neurons, embryos (15.5 days post conceptionem) were obtained from the mating of ATF4 heterozygous mice.

**Primary cortical neurons and cell culture.** Primary neuronal cultures were prepared from the cerebral cortices of mouse embryos, as described previously (55), with minor modifications. The mouse hippocampal cell line HT22 was maintained according to standard procedures (56). Transfection of both cortical neurons and HT22 cells was performed using Lipofectamine 2000 (Invitrogen) according to the manufacturer's instructions. Recombinant arginase was provided by D. Ash (Temple University, Philadelphia, PA).

**Genotyping.** Genomic DNA for PCR was prepared using the DNeasy genomic DNA isolation kit (QIAGEN). The WT alleles were detected using the primer 5′-AGCAAAACAAGACAGCAGCCACTA-3′. The ATF4$^{-/-}$ alleles (neomycin) were detected using the primer 5′-ATATTGCTGAAGAGCTTGGCGGC-3′. As a common reverse primer, we used 5′-GTTTCTACAGCTTCCTCCTCCACTCTT-3′.

**Cell viability/cell death assays.** Cell viability was assessed by propidium iodide uptake and retention of calcein (Invitrogen) using an inverted epifluorescence microscope (Axiovert 200M; Carl Zeiss, Inc.). MTT assay was performed according to the manufacturer's instructions (Promega). In brief, absorbance was measured at 570 nm. From each data point, the reference absorbance measured at 690 nm was subtracted. Finally, values were calculated as the percentage of untreated control cells.

**Plasmids.** The expression plasmids for ATF4WT and dominant-negative ATF4ΔRK (provided by J. Alam, Ochsner Foundation, New Orleans, LA) (37), and the mouse ATF4 5′UTR luciferase construct (D. Ron, New York University, New York, NY) have been previously described. The promoter construct pTRB3 was generated by amplification of genomic mouse DNA using the primers 5′-CTCACTCAGGTGCCTGTAGTGCTCG-3′ and 5′-TCAGCAGAAGCAGCCAGAGGTGTAG-3′, followed by a second round of PCR with the primers 5′-ACACTCGAGAGAGAAACAAATGTGTCATG-3′ and 5′-ACAAAGCTTCTAGAGAGCAAGGAAGAAAG-3′ before cloning into the vector pGL3basic (Promega). The mutant form lacking the 33-bp ATF4 binding site was generated using a site-directed mutagenesis kit (QuikChange; Stratagene). To generate the reporter plasmids with the 33-bp ATF4 binding sequence, the following oligonucleotides were annealed and cloned into pGL3 basic: p33WT, 5′-TCGAGGCAGATTAGCTCAGGTTTACATCAGCCGGGCGGGGATCCA-3′ and 5′-AGCTTGGATCCCCGCCCGGCTGATGTAAACCTGAGCTAATCTGCC-3′; and p33MUT (mutant form), 5′-TCGAGGCAGATTAGCTCAGTCTAAACCTATAGGGGCGGGGATCCA-3′ and 5′-AGCTTGGATCCCCGCCCCTATAGGTTTAGACTGAGCTAATCTGCC-3′. All sequences were verified by automatic DNA sequencing.

**Luciferase assay.** Primary neurons and HT22 cells were transfected with the respective reporter construct along with the pTK-Renilla control (Promega). A dual luciferase assay (Promega) was performed using a bioluminometer (MDS Analytical Technologies), according to the manufacturer's instructions.

**Adenoviruses.** To generate the adenoviruses ATF4WT and ATF4ΔRK, the expression cassettes of each construct were cloned into the shuttle vector ad5 pVQ-K-NpA. The correct sequence was confirmed by automatic DNA sequencing. Virus generation and amplification were performed by ViraQuest. Infection with adenoviruses was performed at a multiplicity of infection (MOI) of 100.

**Gene array analysis.** RNA quantity was assessed with a spectrophotometer (Nanodrop; Thermo Fisher Scientific), and quality was assessed with nanochips (Bioanalyzer; Agilent Technologies). Total RNA was amplified, labeled, and hybridized on arrays (MouseRef-8 Expression BeadChip; Illumina). Data analysis was performed using Bioconductor packages (available at http://www.bioconductor.org; reference 57). Raw data were log2 transformed and normalized using quantile normalization. Analysis of differential expression was performed using a linear model fitting (LIMMA package; reference 58). The obtained p-values were corrected for multiple testing using the false discovery rate method, and a threshold of 0.05 was applied. Microarray data have been deposited in the National Center for Biotechnology Information Gene Expression Omnibus under accession no. GSE10470.

**DNA EMSA.** Crude nuclear extracts were purified by dialysis using Slide-A-Lyzer MINI Dialysis Units (Thermo Fisher Scientific). The following oligonucleotide probes (Invitrogen) corresponding to the ATF4 binding site of the TRB3 gene were used: TRB3WT, 5′-GATTAGCTCAGGTTTACATCAGCCGGGCGGGGA-3′; and TRB3MUT, 5′-GATTAGCTCAGTCTAAACCTATAGGGGCGGGGA-3′. The oligonucleotides were annealed with complementary DNA and radiolabeled with γ-[$^{32}$P]ATP using T4 polynucleotide kinase. After incubation with nuclear extracts, the DNA–protein complexes were resolved in 5% polyacrylamide gels, and the signal was visualized using a PhosphorImager (Fujifilm).

**Chromatin immunoprecipitation assay and PCR amplification.** Formaldehyde cross-linking and chromatin immunoprecipitation were performed as described previously (59). The cross-linked chromatin suspension was sonicated using a Sonicator 3000 (Mosonix). Immunoprecipitation was performed with an anti-myc antibody. DNA–protein cross-linking was reversed, followed by an overnight incubation at 65°C. DNA was isolated by phenol/chloroform extraction and subjected to PCR analysis using the primers 5′-GGTCACAGATGGTGCAATCC-3′ and 5′-AACTGAGCAGCTCTCGGAGTC-3′.

**Glutathione determination using HPLC electrochemical detection and ROS detection using DCF fluorescence.** Concentrations of reduced glutathione were measured using HPLC (PerkinElmer) equipped with an eight-channel coulometric array detector (ESA, Inc.). Cells were lysed in 5% (wt/vol) metaphosphoric acid and centrifuged at 10,000 *g* for 10 min to sediment protein. Cell-pellet precipitates were saved for protein determinations. Glutathione concentrations of supernatant fractions were determined by injecting 5-μl aliquots onto an Ultrasphere 5 u, 4.6 × 250 mm, C18 column (Beckman Coulter), and eluting with a mobile phase of 50 mM $NaH_2PO_4$, 0.05 mM octane sulfonic acid, 1.5% acetonitrile (pH 2.62) at a flow rate of 1 ml/min. Peak areas were analyzed using software from ESA, Inc. Intracellular generation of ROS was determined by DCF. Cortical neurons were seeded in 96-well fluorescence plates. After the treatments indicated in the figures, the cultures were incubated for 45 min with 1.25 μM DCF-$H_2$. Cells were washed with HBSS and read on a plate reader (Fluorometer; MDS Analytical Technologies) at 485-nm excitation and 530-nm emission wavelengths.

**Cerebral ischemia.** Transient focal cerebral ischemia was induced by MCAo using the intraluminal filament method, as previously described (23). Male mice were anesthetized. A small incision was performed in the skin covering the scalp, and a fiber optic probe was glued to the parietal bone and connected to a laser-Doppler flowmeter (Periflux System 5010; Perimed) for continuous monitoring of cerebral blood flow. For MCAo, a heat-blunted black monofilament surgical suture (6-0) was inserted into the exposed external carotid artery, advanced into the internal carotid artery, and wedged into the circle of Willis to obstruct the origin of the MCA. The filament was left in place for 45 min and withdrawn.

**Physiological parameters.** Animal physiology was assessed in ATF4$^{+/+}$ and ATF4$^{-/-}$ mice ($n$ = 3 each). For this purpose, the left femoral artery was cannulated using a polyethylene tube (PE-10; BD Biosciences) to record mean arterial blood pressure. Blood samples were taken for chemical analysis using a hand-held blood analyzer (iSTAT; Abbot Laboratories).

**Quantification of infarct volume.** Coronal brain sections were serially cut in a cryostat (Leica) and stained with cresyl violet to identify viable tissue.

To correct for the effect of edema, the infarcted area was determined indirectly by subtracting the area of the healthy tissue in the ipsilateral hemisphere from the area of the contralateral hemisphere on each section. Infarction volume was calculated by integration of infarct areas measured in 20 equidistant brain sections that encompassed the whole lesion. Volumes from all sections were summed to calculate total infarct volume.

**Cerebral macrovascular morphology.** To assess the morphology of major cerebral blood vessels of the circle of Willis, deeply anesthetized mice were perfused transcardially with a prewarm (37°C) saline solution containing gelatin (20% wt/vol) and India ink (0.25% vol/vol).

**Neurological evaluation.** Neurological scores were assigned the following values: 0, normal motor function; 1, flexion of torso and contralateral forelimb when the mouse was lifted by the tail; 2, circling to the contralateral side when the mouse was held by the tail on a flat surface, but normal posture at rest; 3, leaning to the contralateral side at rest; and 4, no spontaneous motor activity. The inclined plane test measured the time a mouse managed to hold itself on an inclined glass plate angled at 50° before sliding down. The hanging wire test determined the time it took an animal to cross a distance of 45 cm on a freely hanging narrow metal bar.

**Online supplemental material.** Table S1 compares the array data from fibroblasts (11) with the microarray data obtained from neurons. Table S2 summarizes physiological data in $ATF4^{+/+}$ and $ATF4^{-/-}$ mice. Table S3 shows a complete list of all genes differentially expressed after statistical analysis, including p-values and gene ontology information, and a list with the complete gene ontology analysis. Fig. S1 shows measurements of DCF fluorescence in $ATF4^{+/+}$ and $ATF4^{-/-}$ neurons in response to HCA. Fig. S2 shows measurements of cerebral blood flow, body temperature, and blood pressure during MCAo. Online supplemental material is available at http://www.jem.org/cgi/content/full/jem.20071460/DC1.

The authors wish to thank Jawed Alam for providing us with the expression plasmids for ATF4. The ATF4 5′UTR reporter plasmid was a gift from David Ron. David Ash provided us with recombinant arginase. We thank Brett Langley, Ambreena Siddiq, JoAnn Gensert, Alvaro G. Estevez, Jin Son, Bruce Volpe, and Gary Gibson for sharing various materials and for their invaluable advice and encouragement throughout this study. This work was possible because of the outstanding technical support from Hsin-Hwa Lee, Chu-Hui Peng, Lucretia Batten, and Elizabeth Newman.

This study was supported by the W.M. Burke Foundation, by a grant from the National Institutes of Health to Rajiv R. Ratan (NS40591), and by the Dr. Miriam and Sheldon G. Adelson Medical Research Foundation. Philipp S. Lange is a recipient of a postdoctoral fellowship from the Deutsche Forschungsgemeinschaft (LA 1483/1-1) and the Koeln Fortune Program/Faculty of Medicine, University of Cologne (125/2003). Juan C. Chavez is the recipient of a Scientist Development Grant from the Northeast Affiliate of the American Heart Association (0635556T).

The authors have no conflicting financial interests.

**Submitted: 16 July 2007**
**Accepted: 11 April 2008**

## REFERENCES

1. Droge, W. 2002. Free radicals in the physiological control of cell function. *Physiol. Rev.* 82:47–95.
2. Cullinan, S.B., and J.A. Diehl. 2006. Coordination of ER and oxidative stress signaling: the PERK/Nrf2 signaling pathway. *Int. J. Biochem. Cell Biol.* 38:317–332.
3. Beal, M.F. 2000. Oxidative metabolism. *Ann. NY Acad. Sci.* 924:164–169.
4. Banhegyi, G., A. Benedetti, M. Csala, and J. Mandl. 2007. Stress on redox. *FEBS Lett.* 581:3634–3640.
5. Veal, E.A., A.M. Day, and B.A. Morgan. 2007. Hydrogen peroxide sensing and signaling. *Mol. Cell.* 26:1–14.
6. Ryu, H., J. Lee, K. Zaman, J. Kubilis, R.J. Ferrante, B.D. Ross, R. Neve, and R.R. Ratan. 2003. Sp1 and Sp3 are oxidative stress-inducible, antideath transcription factors in cortical neurons. *J. Neurosci.* 23:3597–3606.
7. Liang, G., and T. Hai. 1997. Characterization of human activating transcription factor 4, a transcriptional activator that interacts with multiple domains of cAMP-responsive element-binding protein (CREB)-binding protein. *J. Biol. Chem.* 272:24088–24095.
8. Vinson, C.R., T. Hai, and S.M. Boyd. 1993. Dimerization specificity of the leucine zipper-containing bZIP motif on DNA binding: prediction and rational design. *Genes Dev.* 7:1047–1058.
9. Hai, T., and M.G. Hartman. 2001. The molecular biology and nomenclature of the activating transcription factor/cAMP responsive element binding family of transcription factors: activating transcription factor proteins and homeostasis. *Gene.* 273:1–11.
10. Fels, D.R., and C. Koumenis. 2006. The PERK/eIF2alpha/ATF4 module of the UPR in hypoxia resistance and tumor growth. *Cancer Biol. Ther.* 5:723–728.
11. Harding, H.P., Y. Zhang, H. Zeng, I. Novoa, P.D. Lu, M. Calfon, N. Sadri, C. Yun, B. Popko, R. Paules, et al. 2003. An integrated stress response regulates amino acid metabolism and resistance to oxidative stress. *Mol. Cell.* 11:619–633.
12. Esch, F., K.I. Lin, A. Hills, K. Zaman, J.M. Baraban, S. Chatterjee, L. Rubin, D.E. Ash, and R.R. Ratan. 1998. Purification of a multipotent antideath activity from bovine liver and its identification as arginase: nitric oxide-independent inhibition of neuronal apoptosis. *J. Neurosci.* 18:4083–4095.
13. Ratan, R.R., H. Ryu, J. Lee, A. Mwidau, and R.L. Neve. 2002. In vitro model of oxidative stress in cortical neurons. *Methods Enzymol.* 352:183–190.
14. Ratan, R.R., T.H. Murphy, and J.M. Baraban. 1994. Oxidative stress induces apoptosis in embryonic cortical neurons. *J. Neurochem.* 62:376–379.
15. Ratan, R.R., and J.M. Baraban. 1995. Apoptotic death in an in vitro model of neuronal oxidative stress. *Clin. Exp. Pharmacol. Physiol.* 22:309–310.
16. Ratan, R.R., P.J. Lee, and J.M. Baraban. 1996. Serum deprivation inhibits glutathione depletion-induced death in embryonic cortical neurons: evidence against oxidative stress as a final common mediator of neuronal apoptosis. *Neurochem. Int.* 29:153–157.
17. Lange, P.S., B. Langley, P. Lu, and R.R. Ratan. 2004. Novel roles for arginase in cell survival, regeneration, and translation in the central nervous system. *J. Nutr.* 134:2812S–2817S.
18. Luo, S., P. Baumeister, S. Yang, S.F. Abcouwer, and A.S. Lee. 2003. Induction of Grp78/BiP by translational block: activation of the Grp78 promoter by ATF4 through and upstream ATF/CRE site independent of the endoplasmic reticulum stress elements. *J. Biol. Chem.* 278:37375–37385.
19. Masuoka, H.C., and T.M. Townes. 2002. Targeted disruption of the activating transcription factor 4 gene results in severe fetal anemia in mice. *Blood.* 99:736–745.
20. Ratan, R.R., T.H. Murphy, and J.M. Baraban. 1994. Macromolecular synthesis inhibitors prevent oxidative stress-induced apoptosis in embryonic cortical neurons by shunting cysteine from protein synthesis to glutathione. *J. Neurosci.* 14:4385–4392.
21. Hayashi, T., A. Saito, S. Okuno, M. Ferrand-Drake, R.L. Dodd, and P.H. Chan. 2005. Damage to the endoplasmic reticulum and activation of apoptotic machinery by oxidative stress in ischemic neurons. *J. Cereb. Blood Flow Metab.* 25:41–53.
22. Cho, S., H.H. Szeto, E. Kim, H. Kim, A.T. Tolhurst, and J.T. Pinto. 2007. A novel cell-permeable antioxidant peptide, SS31, attenuates ischemic brain injury by down-regulating CD36. *J. Biol. Chem.* 282:4634–4642.
23. Baranova, O., L.F. Miranda, P. Pichiule, I. Dragatsis, R.S. Johnson, and J.C. Chavez. 2007. Neuron-specific inactivation of the hypoxia inducible factor 1alpha increases brain injury in a mouse model of transient focal cerebral ischemia. *J. Neurosci.* 27:6320–6332.
24. Bagheri-Yarmand, R., R.K. Vadlamudi, and R. Kumar. 2003. Activating transcription factor 4 overexpression inhibits proliferation and differentiation of mammary epithelium resulting in impaired lactation and accelerated involution. *J. Biol. Chem.* 278:17421–17429.

25. Tanaka, T., T. Tsujimura, K. Takeda, A. Sugihara, A. Maekawa, N. Terada, N. Yoshida, and S. Akira. 1998. Targeted disruption of ATF4 discloses its essential role in the formation of eye lens fibres. *Genes Cells*. 3:801–810.
26. Hettmann, T., K. Barton, and J.M. Leiden. 2000. Microphthalmia due to p53-mediated apoptosis of anterior lens epithelial cells in mice lacking the CREB-2 transcription factor. *Dev. Biol.* 222:110–123.
27. Lin, M.T., and M.F. Beal. 2006. Mitochondrial dysfunction and oxidative stress in neurodegenerative diseases. *Nature*. 443:787–795.
28. Sanchez, I., and J. Yuan. 2001. A convoluted way to die. *Neuron*. 29:563–566.
29. Harding, H.P., I. Novoa, Y. Zhang, H. Zeng, R. Wek, M. Schapira, and D. Ron. 2000. Regulated translation initiation controls stress-induced gene expression in mammalian cells. *Mol. Cell.* 6:1099–1108.
30. Rutkowski, D.T., and R.J. Kaufman. 2003. All roads lead to ATF4. *Dev. Cell*. 4:442–444.
31. Siu, F., P.J. Bain, R. LeBlanc-Chaffin, H. Chen, and M.S. Kilberg. 2002. ATF4 is a mediator of the nutrient-sensing response pathway that activates the human asparagine synthetase gene. *J. Biol. Chem.* 277:24120–24127.
32. Novoa, I., H. Zeng, H.P. Harding, and D. Ron. 2001. Feedback inhibition of the unfolded protein response by GADD34-mediated dephosphorylation of eIF2α. *J. Cell Biol.* 153:1011–1022.
33. Lassot, I., E. Segeral, C. Berlioz-Torrent, H. Durand, L. Groussin, T. Hai, R. Benarous, and F. Margottin-Goguet. 2001. ATF4 degradation relies on a phosphorylation-dependent interaction with the SCF(betaTrCP) ubiquitin ligase. *Mol. Cell. Biol.* 21:2192–2202.
34. Yu, V.W., C. Gauthier, and R. St-Arnaud. 2006. Inhibition of ATF4 transcriptional activity by FIAT/gamma-taxilin modulates bone mass accrual. *Ann. NY Acad. Sci.* 1068:131–142.
35. Karpinski, B.A., G.D. Morle, J. Huggenvik, M.D. Uhler, and J.M. Leiden. 1992. Molecular cloning of human CREB-2: an ATF/CREB transcription factor that can negatively regulate transcription from the cAMP response element. *Proc. Natl. Acad. Sci. USA*. 89:4820–4824.
36. Bartsch, D., M. Ghirardi, P.A. Skehel, K.A. Karl, S.P. Herder, M. Chen, C.H. Bailey, and E.R. Kandel. 1995. Aplysia CREB2 represses long-term facilitation: relief of repression converts transient facilitation into long-term functional and structural change. *Cell*. 83:979–992.
37. He, C.H., P. Gong, B. Hu, D. Stewart, M.E. Choi, A.M. Choi, and J. Alam. 2001. Identification of activating transcription factor 4 (ATF4) as an Nrf2-interacting protein. Implication for heme oxygenase-1 gene regulation. *J. Biol. Chem.* 276:20858–20865.
38. Alam, J., and J.L. Cook. 2003. Transcriptional regulation of the heme oxygenase-1 gene via the stress response element pathway. *Curr. Pharm. Des.* 9:2499–2511.
39. Ito, D., J.R. Walker, C.S. Thompson, I. Moroz, W. Lin, M.L. Veselits, A.M. Hakim, A.A. Fienberg, and G. Thinakaran. 2004. Characterization of stanniocalcin 2, a novel target of the mammalian unfolded protein response with cytoprotective properties. *Mol. Cell. Biol.* 24:9456–9469.
40. Yang, X., K. Matsuda, P. Bialek, S. Jacquot, H.C. Masuoka, T. Schinke, L. Li, S. Brancorsini, P. Sassone-Corsi, T.M. Townes, et al. 2004. ATF4 is a substrate of RSK2 and an essential regulator of osteoblast biology; implication for Coffin-Lowry Syndrome. *Cell*. 117:387–398.
41. Averous, J., A. Bruhat, C. Jousse, V. Carraro, G. Thiel, and P. Fafournoux. 2004. Induction of CHOP expression by amino acid limitation requires both ATF4 expression and ATF2 phosphorylation. *J. Biol. Chem.* 279:5288–5297.
42. Ohoka, N., S. Yoshii, T. Hattori, K. Onozaki, and H. Hayashi. 2005. TRB3, a novel ER stress-inducible gene, is induced via ATF4-CHOP pathway and is involved in cell death. *EMBO J.* 24:1243–1255.
43. Satoh, T., S.I. Okamoto, J. Cui, Y. Watanabe, K. Furuta, M. Suzuki, K. Tohyama, and S.A. Lipton. 2006. Activation of the Keap1/Nrf2 pathway for neuroprotection by electrophilic phase II inducers. *Proc. Natl. Acad. Sci. USA*. 103:768–773.
44. Mayumi-Matsuda, K., S. Kojima, H. Suzuki, and T. Sakata. 1999. Identification of a novel kinase-like gene induced during neuronal cell death. *Biochem. Biophys. Res. Commun.* 258:260–264.
45. Lu, P.D., C. Jousse, S.J. Marciniak, Y. Zhang, I. Novoa, D. Scheuner, R.J. Kaufman, D. Ron, and H.P. Harding. 2004. Cytoprotection by pre-emptive conditional phosphorylation of translation initiation factor 2. *EMBO J.* 23:169–179.
46. Ma, L., X. Zhao, and X. Zhu. 2006. Mitosin/CENP-F in mitosis, transcriptional control, and differentiation. *J. Biomed. Sci.* 13:205–213.
47. Shringarpure, R., L. Catley, D. Bhole, R. Burger, K. Podar, Y.T. Tai, B. Kessler, P. Galardy, H. Ploegh, P. Tassone, et al. 2006. Gene expression analysis of B-lymphoma cells resistant and sensitive to bortezomib. *Br. J. Haematol.* 134:145–156.
48. Torigoe, T., H. Izumi, H. Ishiguchi, Y. Yoshida, M. Tanabe, T. Yoshida, T. Igarashi, I. Niina, T. Wakasugi, T. Imaizumi, et al. 2005. Cisplatin resistance and transcription factors. *Curr. Med. Chem. Anticancer Agents*. 5:15–27.
49. Park, H.R., A. Tomida, S. Sato, Y. Tsukumo, J. Yun, T. Yamori, Y. Hayakawa, T. Tsuruo, and K. Shin-ya. 2004. Effect on tumor cells of blocking survival response to glucose deprivation. *J. Natl. Cancer Inst.* 96:1300–1310.
50. Tanabe, M., H. Izumi, T. Ise, S. Higuchi, T. Yamori, K. Yasumoto, and K. Kohno. 2003. Activating transcription factor 4 increases the cisplatin resistance of human cancer cell lines. *Cancer Res.* 63:8592–8595.
51. Dobreva, G., M. Chahrour, M. Dautzenberg, L. Chirivella, B. Kanzler, I. Farinas, G. Karsenty, and R. Grosschedl. 2006. SATB2 is a multifunctional determinant of craniofacial patterning and osteoblast differentiation. *Cell*. 125:971–986.
52. Xiao, G., D. Jiang, C. Ge, Z. Zhao, Y. Lai, H. Boules, M. Phimphilai, X. Yang, G. Karsenty, and R.T. Franceschi. 2005. Cooperative interactions between activating transcription factor 4 and Runx2/Cbfa1 stimulate osteoblast-specific osteocalcin gene expression. *J. Biol. Chem.* 280:30689–30696.
53. Dirnagl, U. 2006. Bench to bedside: the quest for quality in experimental stroke research. *J. Cereb. Blood Flow Metab.* 26:1465–1478.
54. Meisel, C., J.M. Schwab, K. Prass, A. Meisel, and U. Dirnagl. 2005. Central nervous system injury-induced immune deficiency syndrome. *Nat. Rev. Neurosci.* 6:775–786.
55. Siddiq, A., I.A. Ayoub, J.C. Chavez, L. Aminova, S. Shah, J.C. LaManna, S.M. Patton, J.R. Connor, R.A. Cherny, I. Volitakis, et al. 2005. Hypoxia-inducible factor prolyl 4-hydroxylase inhibition. A target for neuroprotection in the central nervous system. *J. Biol. Chem.* 280:41732–41743.
56. Aminova, L.R., J.C. Chavez, J. Lee, H. Ryu, A. Kung, J.C. Lamanna, and R.R. Ratan. 2005. Prosurvival and prodeath effects of hypoxia-inducible factor-1alpha stabilization in a murine hippocampal cell line. *J. Biol. Chem.* 280:3996–4003.
57. Gentleman, R.C., V.J. Carey, D.M. Bates, B. Bolstad, M. Dettling, S. Dudoit, B. Ellis, L. Gautier, Y. Ge, J. Gentry, et al. 2004. Bioconductor: open software development for computational biology and bioinformatics. *Genome Biol.* 5:R80.
58. Smyth, G.K. 2005. Limma: linear models for microarray data. *In* Bioinformatics and Computational Biology Solutions Using R and Bioconductor. R. Gentleman, V. Carey, W. Huber, R. Irizarry, and S. Dudoit, editors. Springer, New York. 397–420.
59. Chavez, J.C., O. Baranova, J. Lin, and P. Pichiule. 2006. The transcriptional activator hypoxia inducible factor 2 (HIF-2/EPAS-1) regulates the oxygen-dependent expression of erythropoietin in cortical astrocytes. *J. Neurosci.* 26:9471–9481.

**Table S1.** Comparison of the gene array data from this study with array data obtained from ATF4-deficient fibroblasts

| | | | | Atf4$^{-/-}$ | | | | Perk$^{-/-}$ | | | |
|---|---|---|---|---|---|---|---|---|---|---|---|
| | | | | Tm | | UT | | Tm | | UT | |
| Product/homology | | GenBank | This study | % of WT | SD | % of WT | SD | % of WT | SD | % of WT | SD |
| **Translation, amino acid import, and metabolism** | | | | | | | | | | | |
| Asns | asparagine synthetase | U38940 | x | 14 | 1 | 24 | 4 | 67 | 11 | 58 | 4 |
| EST | alanyl tRNA synthetase homolog | AI839392 | x | 17 | 1 | 42 | 5 | 67 | 7 | 91 | 5 |
| Slc7a5 | cationic amino acid transporter, y+ system | AB017189 | x | 18 | 1 | 40 | 9 | 40 | 18 | 55 | 13 |
| AAAT | neutral amino acid transporter B | L42115 | | 22 | 1 | 63 | 2 | 62 | 0 | 170 | 85 |
| Mthfd2 | methylenetatrahydrofolate dehydrogenase | J04627 | x | 22 | 5 | 36 | 7 | 87 | 21 | 68 | 8 |
| Rpms7 | phosphoserine aminotransferase homolog | AW122030 | x | 25 | 1 | 32 | 2 | 86 | 37 | 85 | 6 |
| EST | L-3-phosphoserine phosphatase homolog | AI846545 | | 27 | 1 | 52 | 10 | 63 | 3 | 63 | 5 |
| PHAS-I; eIF4Ebp1 | eukaryotic translation initiation regulator | U28656 | x | 27 | 2 | 46 | 1 | 59 | 15 | 64 | 0 |
| Nars | asparaginyl-tRNA synthetase | AW125874 | x | 27 | 1 | 40 | 4 | 52 | 7 | 69 | 14 |
| WRS | tryptophan-tRNA synthetase | X69656 | | 31 | 2 | 44 | 19 | 10 | 3 | 43 | 13 |
| meca39; Bcat1 | branched chain aminotransferase 1 | U42443 | | 32 | 3 | 46 | 7 | 53 | 15 | 66 | 33 |
| EST | threonyl-tRNA synthetase homolog | AI849620 | x | 32 | 6 | 45 | 7 | 58 | 24 | 74 | 11 |
| EST | leucyl-tRNA synthetase homolog | AI844089 | | 33 | 0 | 55 | 9 | 50 | 3 | 68 | 11 |
| Slc3a2 | 4F2 antigen heavy chain, amino acid transporter | X14309 | x | 35 | 2 | 63 | 14 | 86 | 23 | 82 | 8 |
| EST | SYY-Tyrosyl tRNA synthetase homolog | AW122542 | | 40 | 2 | 64 | 3 | 70 | 2 | 89 | 7 |
| EST | isoleucine-tRNA synthetase homolog | AI848393 | | 45 | 0 | 52 | 8 | 83 | 5 | 89 | 14 |
| **Redox or detoxification** | | | | | | | | | | | |
| EST | NADH-cytochrome B5 reductase homolog | AI839690 | | 18 | 1 | 43 | 1 | 19 | 4 | 47 | 14 |
| Cpo | coproporphyrinogen oxidase (hem6) | D16333 | | 32 | 2 | 82 | 39 | 31 | 1 | 47 | 22 |
| Ero1i-pending | ERO1 like, oxidoreductase | AA798624 | | 36 | 1 | 63 | 16 | 57 | 6 | 77 | 24 |
| EST | FKBP13/PDI homolog | AW122851 | | 39 | 6 | 25 | 0 | 81 | 2 | 75 | 0 |
| HO-1, Gmox1 | heme oxygenase | X56824 | x | 45 | 2 | 65 | 5 | 67 | 3 | 69 | 5 |
| **Transcription** | | | | | | | | | | | |
| C/EBPBeta | CCAAT/enhancer binding protein, Beta | M61007 | x | 15 | 4 | 31 | 2 | 29 | 7 | 51 | 17 |
| Prx2 | homeo box of paired rule | X52875 | x | 32 | 2 | 22 | 2 | 52 | 2 | 59 | 6 |
| C/EBRGamma | GPE1-BP (C/EBPGamma) | AB012273 | | 48 | 5 | 65 | 12 | 41 | 2 | 85 | 26 |
| **Secreted or transmembrane protein** | | | | | | | | | | | |
| ptx3 | pentaxin related gene | X83601 | | 7 | 1 | 31 | 14 | 10 | 1 | 32 | 10 |
| Lgals3, L-34 | galactoside-binding lectin; IgE binding protein | X16834 | | 15 | 1 | 18 | 11 | 238 | 120 | 207 | 148 |
| EST | coagulation factor XIIIa homolog | AI839918 | | 19 | 1 | 46 | 8 | 50 | 12 | 71 | 1 |
| X11Gamma | X11gamma protein, mint3, APBA3, Mint-3 | AF070975 | x | 33 | 2 | 46 | 3 | 58 | 3 | 99 | 17 |
| PMP22 | Peripheral myelin protein | Z38110 | x | 37 | 3 | 40 | 1 | 102 | 52 | 52 | 10 |
| Nid2, Ly111 | Nidogen 2; entactin-2 | AB017202 | x | 41 | 14 | 38 | 9 | 154 | 15 | 57 | 10 |
| **Signalling** | | | | | | | | | | | |
| IGFBP-2 | insulin-like growth factor binding protein-2 | X81580 | | 7 | 0 | 9 | 1 | 13 | 7 | 12 | 2 |
| Osmr | Oncostatin M receptor beta | AB015978 | | 26 | 9 | 28 | 9 | 23 | 6 | 66 | 16 |
| EST | EST, GTP-binding protein homolog | AA867773 | | 36 | 6 | 60 | 0 | 88 | 16 | 100 | 10 |
| OPG; Tnfrsf11b | osteoprotegerin, TGFbeta family | U94331 | | 39 | 2 | 42 | 13 | 37 | 4 | 38 | 10 |
| Arhj | Ras homolog gene family | AW121127 | | 44 | 2 | 53 | 4 | 20 | 12 | 19 | 4 |
| Wisp1 | WNT1 inducible signaling pathway protein 1 | AF100777 | x | 46 | 0 | 97 | 11 | 21 | 2 | 27 | 8 |
| Grb10 | growth factor receptor binding protein | U18996 | | 47 | 5 | 50 | 13 | 70 | 8 | 71 | 12 |
| **Miscellaneous** | | | | | | | | | | | |
| Lon | Lon mitochondrial protease homolog | AI838015 | | 2 | 1 | 104 | 109 | 27 | 3 | 195 | 174 |
| PEDF, Serpinf11 | serpin-f1 pigment epithelium-derived factor | AF036164 | x | 10 | 1 | 20 | 3 | 29 | 1 | 37 | 1 |
| Gys | muscle glycogen synthase | U53218 | | 43 | 0 | 50 | 0 | 44 | 3 | 56 | 4 |
| Clic4 | chloride intracellular channel 4 (mitochondrial) | AI849533 | x | 46 | 1 | 70 | 13 | 62 | 3 | 46 | 10 |
| MIBP-1 | myc-intron-binding protein-1 | Y15907 | | 47 | 0 | 69 | 8 | 24 | 33 | 56 | 12 |

An x indicates that the respective gene appears in both datasets as differentially expressed. 42 genes were extracted in the fibroblast array, of which 18 overlap with this study. These are 43% of the 42 genes of the fibroblast data resulting in a high level of significance at the hypergeometric test ($P < 0.00001$).

**Table S2.** Physiological data from $ATF4^{+/+}$ and $ATF4^{-/-}$ mice

| | | WT | KO |
|---|---|---|---|
| before MCAo | | | |
| pO2 | mmHg | 101.33 ± 3.51 | 101.33 ± 2.08 |
| pCO2 | mmHg | 35.33 ± 0.58 | 33.67 ± 0.58 |
| pH | | 7.44 ± 0.02 | 7.39 ± 0.02 |
| $HCO_3^-$ | mmol/l | 22.61 ± 1.28 | 21.84 ± 0.42 |
| Glucose | mg/dl | 87.94 ± 3.78 | 90.38 ± 1.7 |
| Lactate | mmol/l | 1.20 ± 0.11 | 1.2 ± 0.07 |
| mABP | | 73.95 ± 2.56 | 72.95 ± 2.94 |
| mT | $^oC$ | 36.01 ± 0.19 | 35.61 ± 0.4 |
| after MCAo | | | |
| pO2 | mmHg | 97.67 ± 1.53 | 96.67 ± 0.58 |
| pCO2 | mmHg | 32.33 ± 1.53 | 33.67 ± 1.15 |
| pH | | 7.39 ± 0.02 | 7.38 ± 0.03 |
| $HCO_3^-$ | mmol/l | 20.59 ± 0.66 | 20.86 ± 0.57 |
| Glucose | mg/dl | 86.58 ± 5.03 | 85.28 ± 1.05 |
| Lactate | mmol/l | 1.21 ± 0.05 | 1.19 ± 0.05 |
| mABP | | 67.38 ± 2.71 | 66.31 ± 1.11 |
| mT | $^oC$ | 35.49 ± 0.37 | 35.61 ± 0.41 |

Shown are the values for blood gases, pH, levels of bicarbonate, glucose, and lactate, and values for mean arterial blood pressure and body temperature. Measurements were carried out 45 min before and after MCAo for three animals each.